DE-41 (MTS) TAIMOOR, AMEER, HUZEFA, FAISAL

# DEVELOPMENT OF A FORCE SENSOR INTEGRATED SURGICAL INSTRUMENT FOR TELEMANIPULATION BASED MINIMALLY INVASIVE ROBOTIC SURGERY

**COLLEGE OF**
**ELECTRICAL AND MECHANICAL ENGINEERING**
**NATIONAL UNIVERSITY OF SCIENCES AND TECHNOLOGY**
**RAWALPINDI**
**2023**

COLLEGE OF ELECTRICAL AND MECHANICAL ENGINEERING

# DE-41 MTS
# PROJECT REPORT

## Development of a Force Sensor Integrated Surgical Instrument for Telemanipulation based Minimally Invasive Robotic Surgery

Submitted to the Department of Mechatronics Engineering
in partial fulfillment of the requirements
for the degree of

**Bachelor of Engineering**
**in**
**Mechatronics**
**2023**


**Sponsoring DS:**

Dr. Muhammad Mubasher Saleem

**Submitted By:**

Taimoor Shabbir
Ameer Usman
Huzefa Farooq
Faisal Anwar Khan

# ACKNOWLEDGMENTS

This project, paper, and all the research performed for it would not have been possible without the invaluable support of our supervisor, Dr. Mubasher Saleem. Their irreplaceable efforts towards strengthening our endeavors cannot be forgotten. Their knowledge along with their experience helped us to stay on track and achieve what we have achieved. We would also like to express our gratitude towards HEC and the British Council for giving us the opportunity as well as the resources to pursue this idea. Moreover, we would seize this opportunity to appreciate the help and support we received from all our colleagues and friends at the Department of Mechatronics Engineering, CEME, NUST. Their insightful reviews and generosity in more than some instances saved us from several unsought situations.

# ABSTRACT

This project's objective was to create a laparoscopic grasper. that integrates tactile sensors for force and displacement measurement. To achieve this, capacitive force sensors were developed for normal and shear force measurement and were calibrated and validated on an existing laparoscopic surgical tool. The next step involved integrating the tactile sensors with the surgical instrument and developing a data acquisition system that would fit within the size constraints of the instrument. The effectiveness of the developed smart surgical instrument was then validated for tissue stiffness assessment and lump detection. Finally, the surgical system was converted into a telemanipulated system by developing force feedback, allowing for remote operation and control. This project required expertise in mechanical design, sensor development, and data acquisition system design, among other skills.

# TABLE OF CONTENTS

# LIST OF FIGURES

# LIST OF TABLES

# CHAPTER 1- INTRODUCTION

## 1.1.Background

The integration of robotics and computers in minimally invasive surgery (MIS) procedures has brought significant advancements and benefits. These technologies enhance the precision, flexibility, and control of surgical motions, enabling surgeons to perform complex procedures with greater accuracy.

The capability of MIS to scale motions is one of its key benefits, allowing surgeons to make precise movements with reduced tremors. This enhanced dexterity improves surgical outcomes and reduces the risk of complications. Additionally, robotics and computers enable access to difficult orifices that would otherwise be challenging to reach using traditional surgical methods. Robotic-assisted surgery provides surgeons with a wider field of view compared to open surgery, allowing them to visualize the operating site more effectively. This expanded perspective enables surgeons to perform delicate and intricate procedures with improved precision. However, one drawback of MIS is the lack of haptic and tactile feedback. In open surgery, surgeons rely on their sense of touch to assess tissue characteristics such as compliance, viscosity, and surface texture. To overcome this limitation, sensors can be integrated into medical tools to measure instrument-tissue interaction pressures and provide feedback on tissue consistency. The information captured by these sensors is then processed through a signal conditioning circuit and a microcontroller. The microcontroller analyzes the data and generates corresponding outputs that can be transmitted to a tactile display on the surgeon's hands. Actuators within the display provide tactile feedback, allowing surgeons to perceive the physical properties of the tissue being manipulated.

## 1.2.Problem Statement

In minimally invasive surgery and telemanipulation-based robotic surgery, the lack of accurate haptic feedback poses a challenge for surgeons. Without the ability to feel the surfaces they are interacting with, such as human tissue or organs, surgeons may inadvertently apply excessive force, potentially causing harm to the patient. To address this issue, this project aims to develop a smart surgical tool that integrates tactile sensors and haptic feedback. By incorporating tactile sensors into the tool, it becomes capable of capturing detailed information about the surface being touched or manipulated. These sensors can detect properties such as hardness, softness, and surface patterns. The signals captured by the tactile sensors are then processed and translated into haptic feedback, which is provided to the surgeon. This feedback allows the surgeon to perceive the characteristics of the tissue or organ being operated on, providing a more accurate sense of touch. With this enhanced haptic feedback, surgeons can better understand the nature of the surface they are interacting with, enabling them to apply the appropriate amount of force and make more informed decisions during the procedure.

## 1.3.Design

In this project, we have designed a smart laparoscopic tool that allows you to detect the magnitude of force being applied in any laparoscopic surgery using haptic feedback. Haptic feedback generally means to get information (feedback) about anything through touch. During normal laparoscopic surgeries, the surgeon does not get a sensation of the force being applied on any tissue inside the patient's body which increases the chances of tissue damage, blood loss, and ultimately slow recovery. Our Designed laparoscopic tool increases the safety of any laparoscopic surgery by reducing the chances of problems that occur in normal laparoscopic surgery. Apart from the detection of the magnitude of force, surgeons also get information about the stiffness of the tissue that needs to be treated. A sensor placed between the jaws of the tool detects the force which is then passed through a signal conditioning system and transferred to a microcontroller. The microcontroller collects information, analyzes it, and switches on the respective vibratory motors so that the surgeon feels vibrations and knows about the amount of force applied.

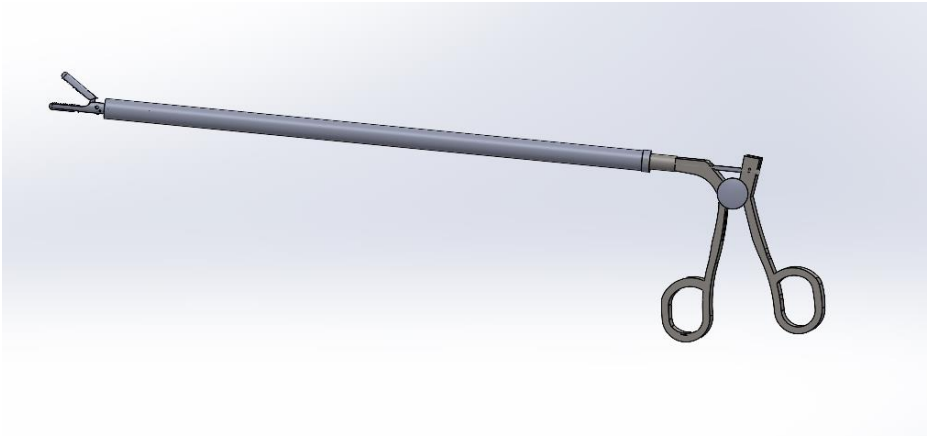

Figure 1. Laparoscopic tool

The mechanism of the laparoscopic tool is based on a single-action grasper. One of the jaws is fixed while the other is movable. It has three major parts one is the handle from where the surgeon carries the tool and applies force, the second one is the internal rod that transfers force from the surgeon's end to the gripping end and the last one is the grasper jaws in which sensor is integrated and that grasp the tissue inside patients' body and perform the required task.

## 1.4.Objective

The main objective of the project is to design an efficient haptic feedback approach by which the user can easily differentiate between surfaces. It can further be divided into multiple objectives:

i. Develop a surgical instrument that integrates tactile sensors into its design for minimally invasive surgery.

ii. Increasing the accuracy and sensitivity of force sensors to ensure the proper haptic.

iii. Provides real-time feedback to the surgeon to ensure the safety and efficiency of the surgical procedure.
iv. Develop a robust signal conditioning and data acquisition system to process and analyze the sensor data.
v. Integrate the angle sensor with the force sensors to detect stiffness in the tissue with high accuracy.
vi. Provide user-friendly software interfaces and intuitive visualization tools to help surgeons interpret and analyze the sensor data.
vii. Offer comprehensive training and support to ensure the proper installation, calibration, and maintenance of the sensor system.
viii. Improve surgical accuracy and safety, reduce surgical errors and ultimately improve patient outcomes.
ix. Low cost, indigenous tool for various applications.

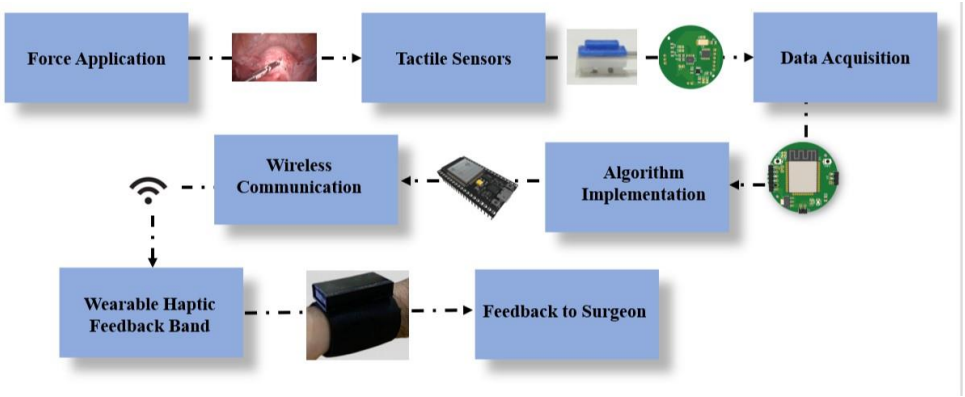


Figure 2. Flow diagram of working of Smart Surgical Tool

## 1.5.Scope

In minimally invasive surgery and telemanipulation-based robotic surgery, the lack of accurate haptic feedback poses a challenge for surgeons. Without the ability to feel the surfaces they are interacting with, such as human tissue or organs, surgeons may inadvertently apply excessive force, potentially causing harm to the patient. To address this issue, this project aims to develop a smart surgical tool that integrates tactile sensors and haptic feedback. By incorporating tactile sensors into the tool, it becomes capable of capturing detailed information about the surface being touched or manipulated. These sensors can detect properties such as hardness, softness, and surface patterns. The signals captured by the tactile sensors are then processed and translated into haptic feedback, which is provided to the surgeon. This feedback allows the surgeon to perceive the characteristics of the tissue or organ being operated on, providing a more accurate sense of touch. With this enhanced haptic feedback, surgeons can better understand the nature of the surface they are interacting with, enabling them to apply the appropriate amount of force and make more informed decisions during the procedure.

# CHAPTER 2- LITERATURE REVIEW

## 2.1.Motivation

In this era of robotics and technology everything is moving towards automation. Automobile sector is the best example of that, the first ever car was very simple, and the latest auto driven car shows the evolution in automation. Similarly, we can see the change in industries, smartphones, and medical equipment. Currently, research work is going on to widen the scope of robotics. Surgery is a medical procedure in which a patient's body is cut open to allow a surgeon to replace, remove, or repair an unhealthy or broken portion. Surgery is a vital act, but many procedures result in unfavorable adverse effects.

Figure 3. Intuitive surgical Da Vinci robotic surgery system [31]

## 2.2.Haptic Feedback

Haptics, which includes cutaneous (tactile) and kinesthetic (force) input, is the word used to describe touch feedback. As opposed to minimally invasive robotic surgery (MIRS), where the surgeon is not directly controlling the tool, minimally invasive surgery (MIS) practitioners may feel the tool-tissue contact of the instrument with the patient's body [1]. During the process, this gives the surgeon feelings that relate to tissue damage, suture straightness, and job completion time.[2].

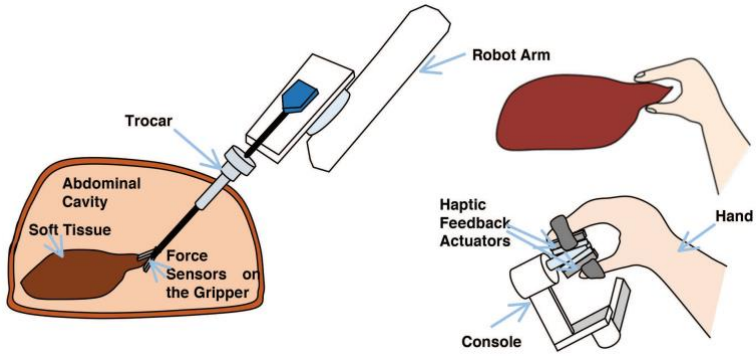


Figure 4. Schematic diagram of the multi-fingered palpation in robot-assisted minimally invasive surgery [44]

### 2.2.1. Importance of Haptic Feedback

When asked whether force feedback is necessary during robotic surgery, a surgeon will almost probably answer "yes." This response's intuitive foundation might not be immediately obvious. High-fidelity force information may not be required for all surgical activities, as demonstrated by the frequent use of hand-held instruments by surgeons for a range of minimally invasive procedures [3]. Additionally, surgical robots like the DaVinci system are being used by MIS more and more, but until recently, these systems lacked trustworthy force feedback [4].

Surgical robotic systems enable a 30% decrease in assignment completion time and a 60% reduction in error, while also reducing patient stress, recuperation time, energy usage during the procedure, and total cost. Without haptic input, robotic surgery causes surgical operations to be unclear [5].

## 2.3.Minimally Invasive Robotic Surgery (MIRS)

One of the most important tasks during surgeries is to reduce the size of cuts or incisions, so that there is minimum damage to human body. In this regard the best surgical method is known as minimal invasive surgery. During this process, surgeons make small incisions through which surgical instruments are inserted. The surgeon gets feedback by using different cameras and performs required operations to treat patient [6].

### 2.3.1. Types of Minimally Invasive Surgery

There are various types of Minimal invasive surgeries the most important among them are:

i. Laparoscopic surgery
ii. Robotic surgery

#### 2.3.1.1 Laparoscopic Surgery

In laparoscopic surgery, surgeons make a small incision into abdominal cavity through which surgical instruments are inserted and operation is performed. A camera inserted along with other surgical tools is used to get view of inner body [7].

#### 2.3.1.2 Robotic Surgery

Robotic surgery provides a 3D view to surgeon of surgical site and perform operation with much precision, control and flexibility although its practical application is less due to expense, transmission delay and medical and legal issues [8].

### 2.3.2. Diseases Treated by Minimally Invasive Surgeries

Some of the common diseases which are treated by minimal invasive surgery are:

i. Adrenalectomy
ii. Brain surgery
iii. Colectomy

iv. Gallbladder surgery
v. Heart surgery
vi. Hiatal hernia repair
vii. Kidney transplant

### 2.3.3. Advantages of Minimally Invasive Surgery

Some of the advantages of minimal invasive surgery are following:

i. Less trauma because the surgeon typically does not cut muscle or other tissue to reach the surgical site [6]
ii. Some procedures can be performed on an outpatient basis, which may reduce or even eliminate hospital stays [6]
iii. Less scarring [6]
iv. Safe due to less blood loss and lower risk of infection [6]

### 2.3.4. Risk Factors

i. Communication and environmental failures [11]
ii. There can be complications like bleeding, infection and injury, although its risks are lower
iii. Special training required [11]

### 2.3.5. Surgical Tools Used in MIRS

As it is mentioned earlier two types of minimal invasive surgeries are common. There are various tools that are used in these surgeries, every tool has its own features and benefits. Some of them are mentioned below.

The tools which are disposed of after usage are disposable tools. These tools are convenient because they reduce the time of interoperation preparation, however they are less precise and can increase cost of procedure up to a factor of $10^5$ [9].

In contrast, reusable instruments are precise and can be used multiple times, they are also less costly.

These instruments are both reusable and disposable [9].

Figure 5. Laparoscopic dissectors [9],[42]

Figure 6. Laparoscopic dissectors [9],[42]

In such instrument sensors are equipped at the end of normal forceps that can be used to detect normal force as well as forces in X, Y, Z axes [12].

Figure 7. Laparoscopic forceps with force feedback [12]

It is the tool used to get hold of anything. Laparoscopic graspers should have great mechanical efficiency and constant force transfer. [10].

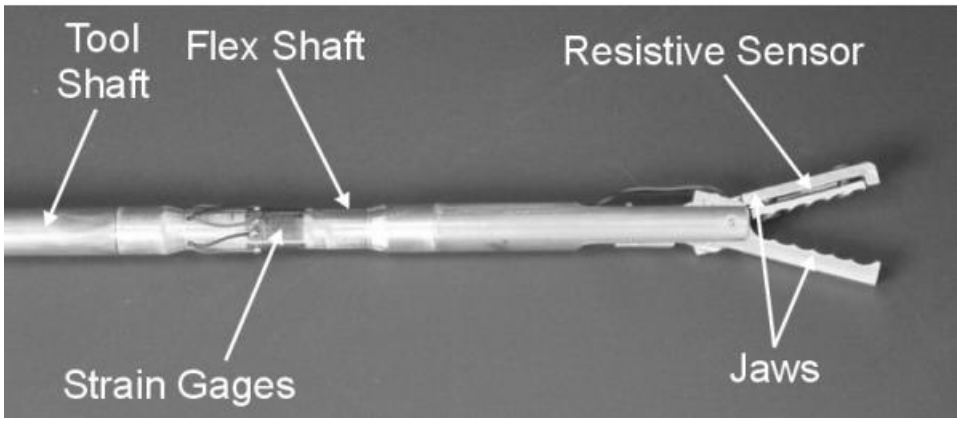


Figure 8. Laparoscopic automated grasper [15]

## 2.4.Robot Surgical Tools

When laparoscopic tools are attached to some type of manipulator and then manipulator is controlled by some controller, such systems are called robotic surgical systems. The most popular one is Da Vinci [13].

## 2.5.Sensor Integration on Laparoscopic Surgical Tool

As various types of sensors are used to get feedback, their integration should be done according to their function. Some of the most common type of sensors that are used to deliver information along with their integration are mentioned as follows:

### 2.5.1. Force Sensors

These sensors deliver vital information about how much force must be exerted on the inner body parts so that safe operation can be formed. From the tip of tool information is delivered to controller using wired/wireless communication. Controller after receiving signal, sends an appropriate signal to actuators so that surgeon gets required information [14].

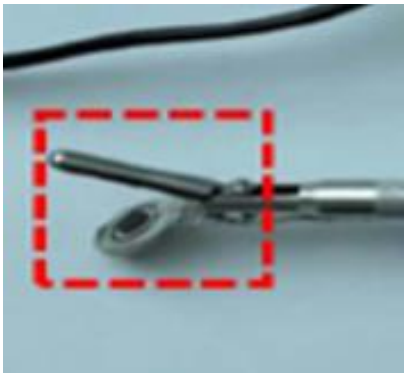

Figure 9. Force sensor [14]

### 2.5.2. Angle Sensors

Angle sensors are often used to detect the angle of grasping. These sensors are attached at the holding side of grasper. Information is transferred from sensor to controller which father represents the information on LCD or sends specific signal to actuators for dedicated operation [14].

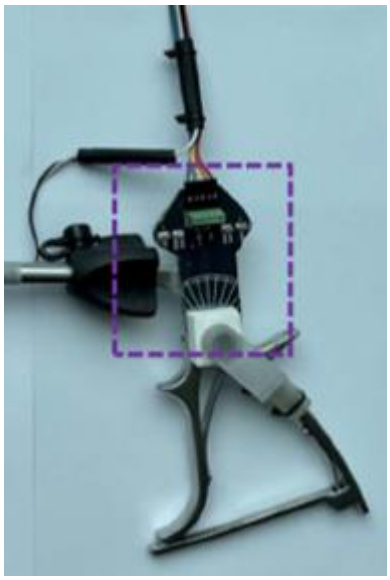

Figure 10. Angle sensor [14]

### 2.5.3. Fiber Bragg Grating Sensor (FBGs)

To sense clamping force an FBG is used along central line with two point passing configuration. For this purpose, the FBG is stretched with a pre tensioning force, and the horizontal strain is measured at the two ends that passes through midline. When grasper clamp tissue, surface of clamping flexure deform due to which uniform strain is produced linearly. Now the grasping force and strain can be calculated by using relationship [23].

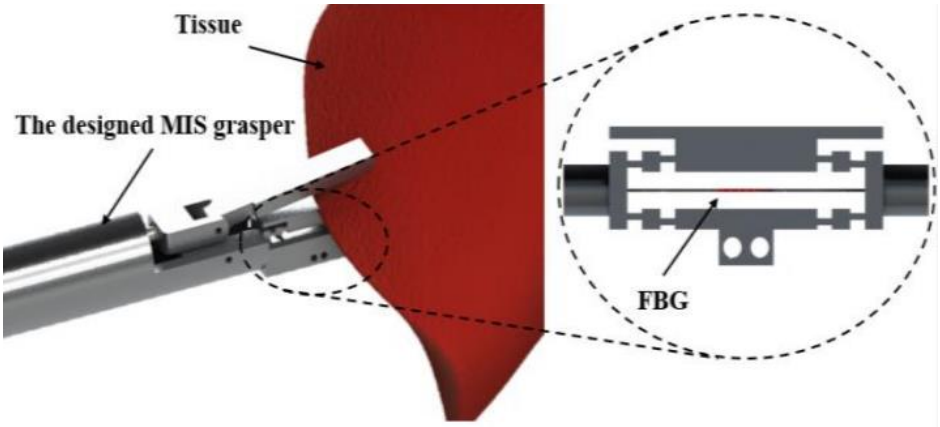


Figure 11. FBGs in laparoscopic tool [23]

### 2.5.4. Capacitive-Type Sensors

These sensors are used to measure both normal and shear forces. When the distance between any two electrodes decreases, the capacitance changes whose value is used to determine the normal shear force using transducer and other circuitry. The data is sent to controller which in return sends signal

to actuators to give information about force to surgeon [41].

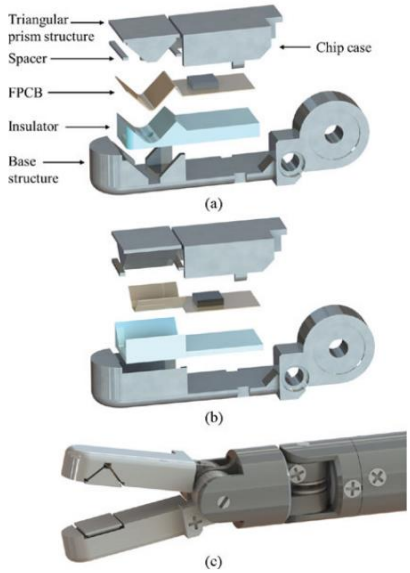


Figure 12. Capacitive type sensor integrated on grasper [41]

## 2.6.Tactile Sensing

The second aspect is force feedback, which involves providing the surgeon with a sense of touch and feedback regarding the force applied to the tissue This allows the surgeon to perceive the resistance and pressure exerted on the tissue, enabling them to have a better understanding of the tissue properties and make more precise and controlled movements during the procedure. [22].

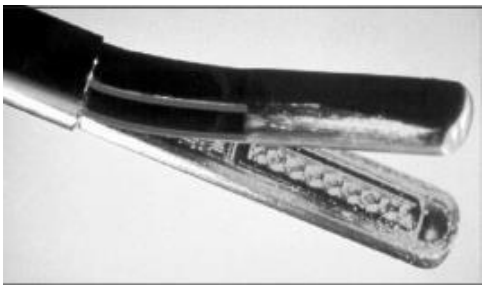

Figure 13. Forceps with integrated sensors [22]

### 2.6.1. Tactile Sensors

A tactile sensor system consists of three essential components: the tactile sensor itself, the signal processing unit, and the output interface. The signal processing unit receives and analyzes the sensor data, applying various techniques to enhance its accuracy and reliability. [25] Finally, the output interface presents the processed tactile information in a usable form, whether through visual displays, haptic feedback devices, or data output for further analysis or system control. Together, these components enable the

measurement and interpretation of physical contact events, providing valuable insights into the properties and characteristics of the objects or surfaces being sensed.

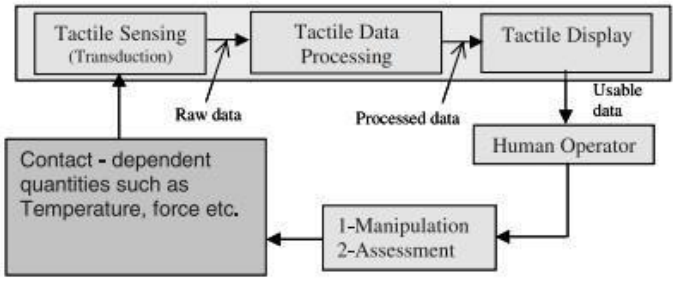


Figure 14. Block diagram of a tactile sensing system [25]

Tactile Sensors will be the focus of this part. According to the analysis performed by Kattavenos et al. [19], the piezoresistive method i.e., pressure leading to resistance change, was the most suitable for this application but that will be evaluated later in this paper. Tactile sensors can provide a more delicate measurement. Although these sensors provided a sense of touch, their principal technological approach suffers the same integration and sterilization issues, as the transducer must be located near to the device tip in direct contact with organs. Furthermore, the size of these systems is extremely large due to the requirement for peripheral electrical components and communication lines. [22] Electrical or optical concepts have largely guided the development of tactile sensors for MIS applications.

### 2.6.2. Elastomer Based

Piezoresistive devices work on the principle that the contact and force between the touched body and sensing layer of the device, which is made up of carbon or silver impregnated rubber, causes an increase in conductivity based upon the increase in the amount of the conductive particles [20].

The structure of capacitive tactile sensors consists of two conducting layers separated by a silicon-rubber-based dielectric. The application of force reduces the distance between the conductive surfaces, increasing capacitance. This can be used to measure the spatial distribution of pressure by measuring capacitances at crossing points [21]. Some properties of rubber such as viscoelasticity limit dynamic range and properties like creep and hysteresis put constraints on the size. Conductive rubber also introduces noise [29].

### 2.6.3. Silicon Based

A sensor based in silicon capacitive transduction was proposed by Chun and Wise [27] containing an 8x8 array tactile imager. It consists of a metallized pattern on an opposing glass substrate to which a thin, boron-doped silicon diaphragm is electrostatically bonded. The transducer plates are isolated

using silicon dioxide making them isolated row lines. It uses thick silicon rims making it not suitable for high density use because of size constraints. The tactile imager was further modified by Suzuki et al. [28] by implementing a double supported bridge structure which is supported only on two sides hence reducing die are and the bridge area requires lesser space than the diaphragm making a 32x32 array possible.

In order to create a sensor, Wolfenbüttel and Regtien [29] used surface micromachining to create a bridge microstructure on top of a silicon wafer covered in a composite silicon dioxide and silicon nitride coating.

There are three types of sensing principles that are used for tactile sensing that are used in obtaining haptic feedback for laparoscopic graspers for minimally invasive surgery. These principles are as follows:

i. Piezoresistive sensing principle
ii. Capacitance change sensing principle
iii. Fiber Bragg Grating principle

## 2.7.Piezoresistive Sensing Principle

Piezoresistive Effect is defined as the change in resistance of semiconductors and conductors due to pressure or strain applied on them [16]. The magnitude of the effect is proportional to the fractional change in resistance $GF \propto \frac{\Delta R}{R_o}$. Where GF represents Gauge Factor that gives the performance magnitude of the piezoresistive effect for the material [16], $\Delta R$ represents the change in resistance and $R_o$ represents the resistance of the material under zero mechanical deformations. This change occurs due to the change in geometrical shape of the material [16, 17].

$$\frac{\Delta R}{R_0} = (1 + 2\nu)\epsilon + \frac{\Delta \rho}{\rho} \quad (1)$$

Where ν represents the Poisson's ration, ϵ represents the strain, $\frac{\Delta \rho}{\rho}$ represents the resistivity change of material [17].

In this configuration a slight change in resistance can be detected by an output voltage signal $V_0$, this output signal is then amplified using differential amplifier configuration to get a detectable signal [18].

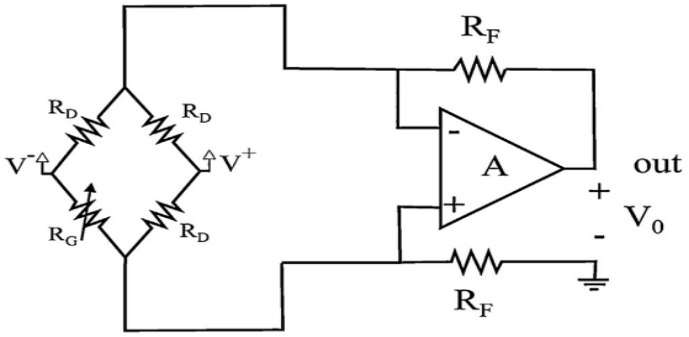


Figure 15. Differential amplifier with Wheatstone bridge [18]

The sensors used in the application such as the haptic feedback for Minimally Invasive Robot assisted Surgery (MIRS) are strain-gauges and Force Sensing Resistors (FSR) pressure sensors [19].

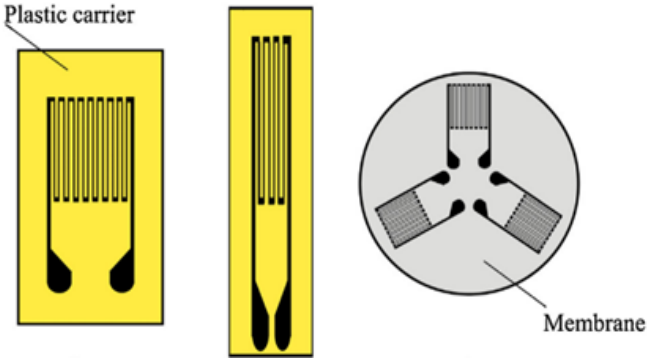


Figure 16 Different configurations of strain-gauges [19]

Figure 17 Different Force Sensing Resistors (FSR) pressure sensors [43]

## 2.8.Capacitance Change Sensing Principle

The capacitance C between two electrodes depends upon several factors such as the overlapping area $A$ between the electrodes, separation $d$ between them, dielectric constant for air $\epsilon_0$ and $\epsilon_r$ represents the relative permittivity of the dielectric medium [20].

$$C = \frac{\epsilon_0 \epsilon_r A}{t} \qquad (2)$$

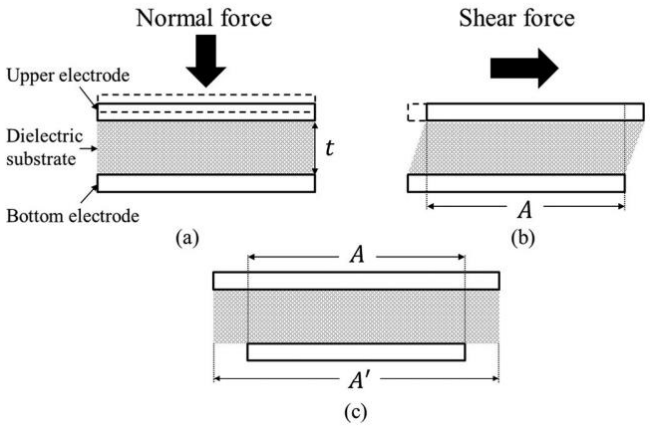


Figure 18. (a) Capacitive sensor under normal force causing change in thickness. (b) Sensor under shear causing change in A. (c) This configuration restricts changes in A and only thickness changes and area remains the same (it only measures Normal

In Capacitive sensors used in Laparoscopic graspers, one of the electrodes in movable, that allows the applied force to change the distance between the electrodes, which creates a capacitance change due to change in thickness which then is calibrated to calculate the magnitude of the applied force [20].

The next step is to read the capacitance changes that occur when there is a change in any parameter of the sensor, for that CDC (Capacitance to Digital Converters) are used, the bridge configuration for CDCs is shown [21].

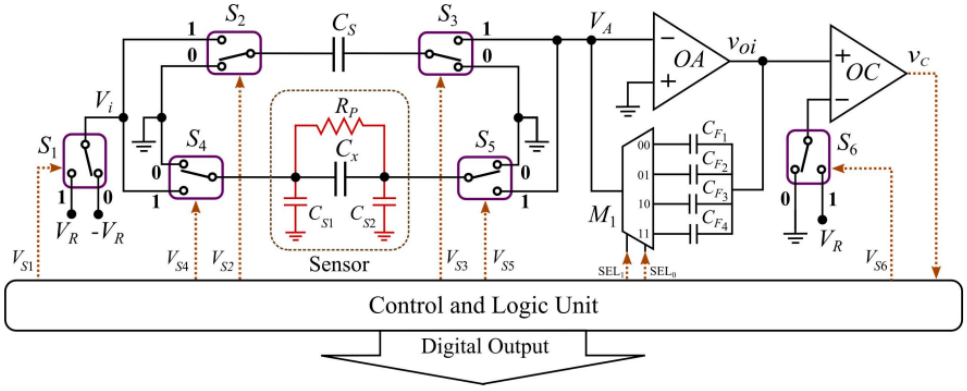


Figure 19 Schematic of a capacitance-to-digital converter (CDC) [21]

Where $C_x$ is the sensing capacitor with internal non-ideal parameters $R_p, C_{s1}, C_{s2}$ as parasitic resistance and stray capacitances, respectively. This CDC converts the capacitance changes into a digital output that can be used for calculations of force feedback [21].

There is no capacitive sensor available commercially that fits the dimensional criteria for our application, therefore these sensors will have to be designed by the FYP group members.

## 2.9.Fiber Bragg Grating Principle

FBG (Fiber Bragg Grating) works on the bases of periodic refraction modulation whenever there is a strain interference in the FBG, the wavelength of light that satisfies the Bragg interference condition is reflected and the rest are transmitted. The shift in the reflected wavelength ($\Delta\lambda_B$) provides information about the strain [22].

$$\frac{\Delta\lambda_B}{\lambda_B} = (1 - p_e)\epsilon_{FBG} \quad (3)$$

Where $\frac{\Delta\lambda_B}{\lambda_B}$ represents the fractional Bragg wavelength shift, $\epsilon_{FBG}$ is the interfering strain in the grating and $p_e$ represents the effective photo-elastic coefficient.

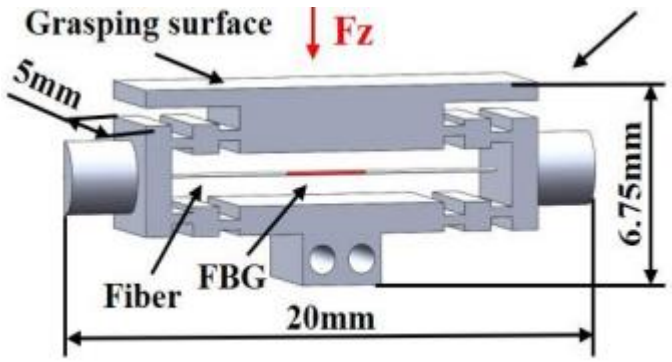


Figure 20 A structural design for forceps of laparoscopic grasper with a suspended FBG for force measurement [23]

The Fiber grating is suspended in a mechanical structure and that mechanical structure is designed differently based on the application. For MIRS a proposed design for laparoscopic grasper is shown (Figure 20) [23] along with another design for Structural Health Monitoring (SHM) (Figure 21) [22].

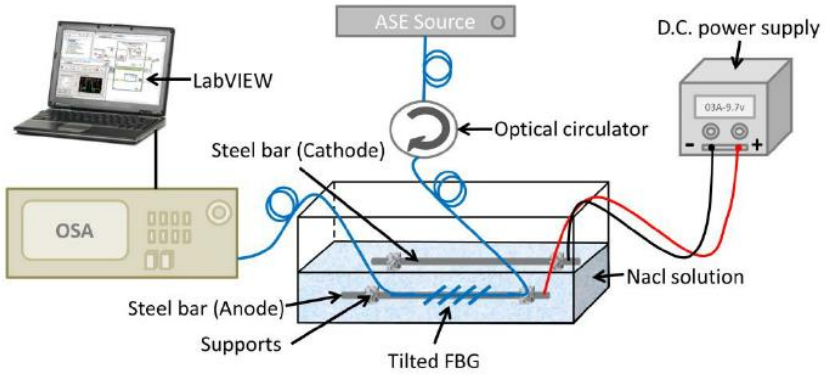


Figure 21 Schematic of a tilted FBG sensor to the rebar and impressed current technique setup

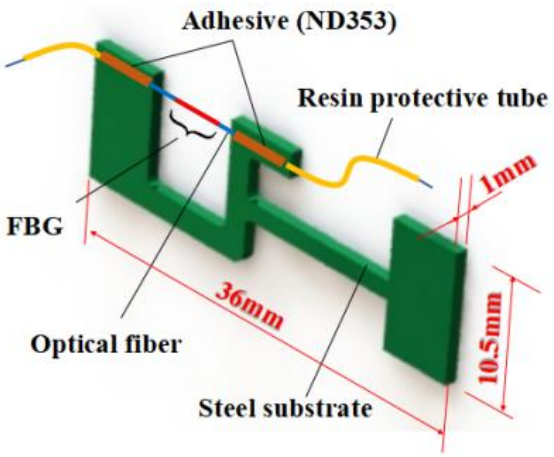


Figure 22 A structural design for the measurement of crack propagation in buildings for SHM [22]

The experimental setup for FBG data acquisition requires an FBG interrogator which is required for the conditioning of the signals, a specially designed DAQ card, and an Interface Power Supply. The interrogator is very costly, that is why in our application FBG cannot be utilized [23].

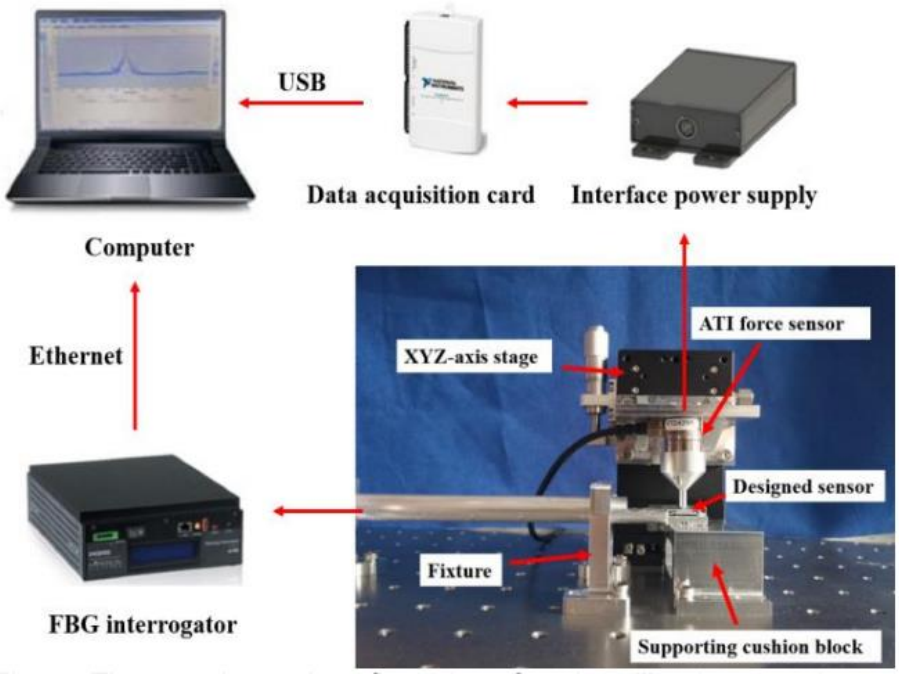


Figure 23. Experimental setup for FBG sensing [23]

## 2.10.Telemanipulation

Telemanipulation systems are a type of robotics that allows the operator to work remotely using a computerized human-machine interface [24]. A sophisticated electromechanical system known as telemanipulation consists of a master and

slave device connected by communication lines. A human operator (the master) and the environment (the slave) are interfaced with the entire system., see Fig. 3 [25].

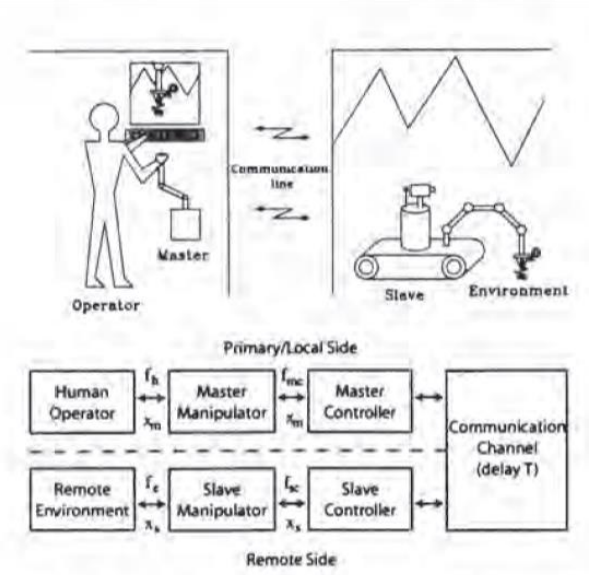


Figure 24. A tele-manipulator and its block representation. variables at the master and slave sites are denoted by the subscripts m and s, respectively [25]

### 2.10.1. Telemanipulation Controls

The telemanipulation controls can be divided into two main categories:

i. Unilateral telemanipulation
ii. Bilateral telemanipulation

#### 2.10.1.1 Unilateral Telemanipulation

Position data is only transmitted in one direction, from the operator to the remote environment.


Figure 25. Unilateral telemanipulation [26]

#### 2.10.1.2 Bilateral Telemanipulation

Signals must be returned to the master side operator to provide more information about the distant environment. As a result, information (such as location, velocity, and/or force) travels both ways between the operator and the environment during bilateral telemanipulation control. The reflected signal affects the receiving-end manipulator's input torque. Figures 3a and 3b compare two bilateral control strategies, one based on position and the other on force. [26].

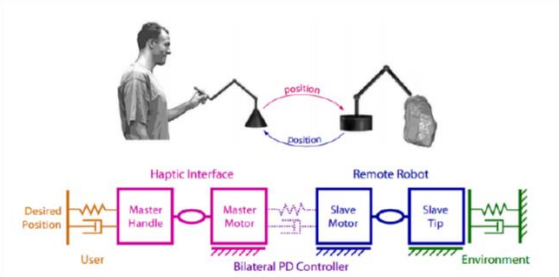


Figure 26. Bilateral telemanipulation (position feedback) [26]

### 2.10.2. Robotic Surgeries

Telemanipulation is used in robotic surgery to precisely control the movement of surgical robots. Motion Scaling can let surgeons manipulate surgical tools precisely to the millimeter [27]. In terms of postoperative discomfort, recuperation time, and total medical care expenses, using robotic technology in minimally invasive surgery (MIS) provides various advantages [28]. The force sent back to the surgeon during routine surgical maneuvers is so minimal that it has no influence on perception or performance, even though commercially available robotic surgery systems offer direct haptic feedback. [30].

### 2.10.3. Haptic Feedback in Telemanipulated Robotic Surgeries

Haptic feedback in robot-assisted minimally invasive surgery aims to create "transparency," which implies that the surgeon should feel as though his own hands are directly touching the patient rather than manipulating a remote apparatus [32]. Humans may manipulate objects remotely via telemanipulation, however when the amount of (haptic) input is restricted, work performance and needed time deteriorate. Another strategy to enhance teleoperated jobs is to provide haptic shared control, where the operator is supported by guiding forces applied at the master device.[33].

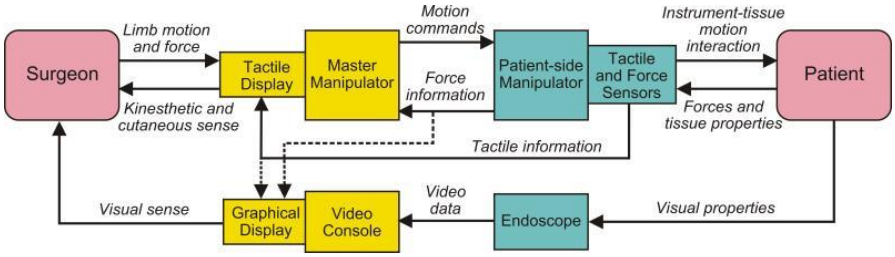


Figure 27. The main components of a teleoperated robot for minimally invasive surgery with haptic feedback [32]

Haptic feedback for RMIS is presently being developed and assessed in engineering labs, and additional work is required before these methods are prepared for clinical testing. A developed natural haptic feedback system, shown in Figure 6, encodes tactile information similarly to the neurological system. [34].

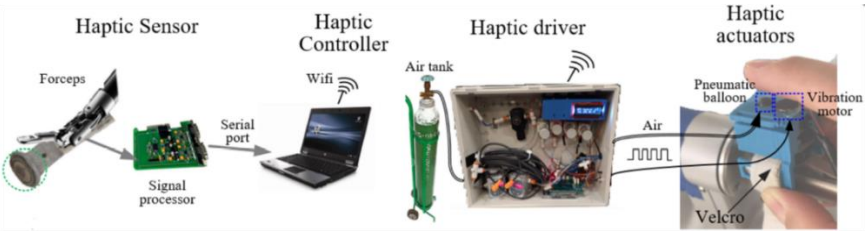


Figure 28. Block diagram of the hardware of haptic feedback system for the surgical robot [34]

### 2.10.4. Frameworks Used in Telemanipulation

#### 2.10.4.1 Virtual Fixture

To enhance human performance in both directly and remotely controlled jobs, a virtual fixture is an augmented sensory information overlay that is overlaid on a user's perception of a real-world environment. Virtual fixtures (VFs) enhance human operator performance in teleoperation circumstances. However, it might be challenging to create VFs, particularly in unstructured situations [35]. Virtual fixtures can speed up and improve operations. Virtual fixtures seek to benefit from the precision of robotic systems while preserving some operator control [36].

#### 2.10.4.2 Electromyography in Robotic Telemanipulation

By deducing human intention and translating it to robot control, electromyography is employed in robotic applications as a communication channel between a person and a robot [37]. One of the most natural human-machine interface alternatives is electromyography (EMG), which enables the user to operate a robot arm and hand system using their own natural arm movements and gestures. EMG-based control also frees up the user's hands so they may engage with the teleoperated machine while carrying out other chores [38].

#### 2.10.4.3 Teleoperated-Autonomous Shared Control System

In a hybrid of teleoperated and autonomous modes, an operator and an autonomous agent can cooperate to perform a job. This is known as a teleoperated-autonomous shared control method. In such contexts, the outcome of the operation benefits not only from the operator's supervision and decision-making skills, but also from a noticeably lower completion time and maybe improved precision because of the autonomous mode. [39].

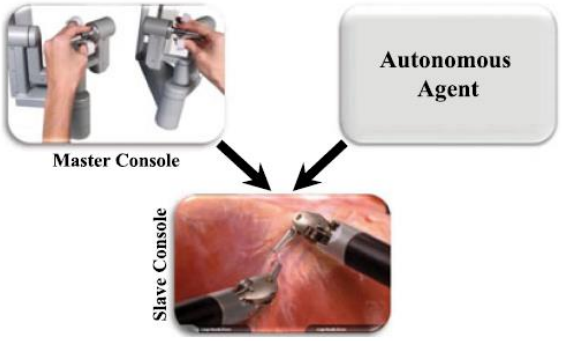


Figure 29. Schematic representation of a TASC system for surgical procedures [39]

The master slave topology is utilized in TASC systems. It is used because the master mimics the slave's movements, addressing many of the problems with traditional control techniques, such as improved ergonomics, the elimination of hand trembling, and reduced time consumption. The correct hardware is then used to recreate this feedback at the master end, producing the precise force or tactile feedback. [40].

## 2.11.System Integration

Combining widely available sensors with a multipurpose laparoscopic grasper. As surgeons use long surgical devices to get into human tissues through tiny incisions, there is an astounding variety of readily available laparoscopic equipment on the market, each designed for a unique purpose and surgical procedure. The forceps end effector of choice features two 6 mm wide gripping jaws, and the opening angle of the tool may be manually adjusted using the handle. To measure the grabbing force and angle, a developed capacitive sensor was installed on the laparoscopic grasper [14].

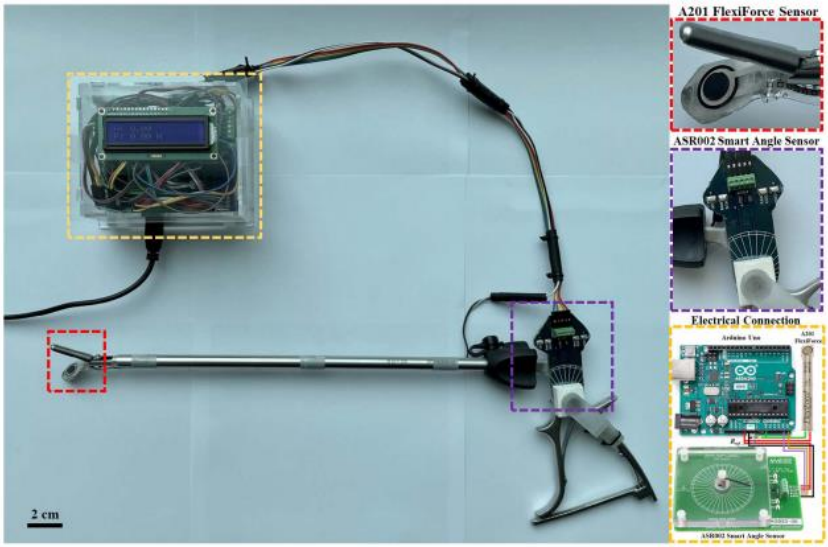

Figure 30. A smart surgical tool for force feedback and lump detection [14]

# CHAPTER 3- METHODOLOGY

## 3.1.Sensor

Our study commenced with an extensive literature review to examine previous research conducted on haptics. We thoroughly examined the design and implementation of the preceding studies. After careful consideration, we devised our own design by incorporating elements from various sources that met our specific requirements. The initial step involved selecting a suitable sensor for the laparoscopic grasper. Since our objective was to measure force in both normal and shear directions, conventional force and flex sensors proved inadequate. Additionally, the sensors available in the market lacked the necessary sensitivity and resolution to provide us with precise results. Consequently, we made the decision to fabricate our own sensor based on a design outlined in reference [45]. A top the electrodes, an elastomer dome is placed to generate a change in capacitance that can be utilized to determine the applied force. To achieve a broad displacement range, the initial separation between the upper and lower plates is adjusted using electromechanical simulations.

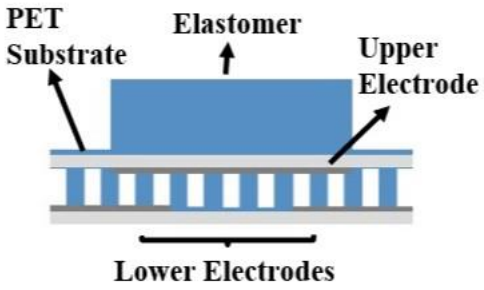


Figure 31. Schematic design of capacitive sensor

### 3.1.1. Ink-Jet Printing method

The initial design of the sensor was fabricated using the inkjet printing technique, which yielded precise results. However, it encountered a few challenges related to the conductivity of the printed electrodes. Over time, the conductivity of the ink varied, leading to fluctuations in the values of capacitance change. Another issue arose when connecting the sensor to the data acquisition system, as only Flexible Printed Circuit (FPC) connectors and cables could be used. This limitation stemmed from the fact that the silver ink-printed electrodes could not be soldered. To address these challenges, we needed to explore alternative methods.

### 3.1.2. Copper-Tape method

In the alternative approach, we replaced inkjet printing on a PET substrate with the utilization of copper tape on the same substrate. The electrodes were formed through the etching process applied to the copper material. This alternative method effectively resolved the two previously mentioned issues.

Firstly, the use of copper eliminated the problem of conductivity variations over time. Unlike the ink used in inkjet printing, copper maintained its consistent conductivity properties. Secondly, soldering the wires to the copper electrodes became feasible, overcoming the limitation encountered with the previous design. Furthermore, this modified design exhibited enhanced accuracy, resulting in more precise measurement outcomes. As a result, we adopted this final design for our sensor.

i. On the upper electrode there is 5 mm by 7 mm hard elastomer pyramid shape dome with height of 2mm, it equally disturbs the force to upper electrode which displaced the upper electrode which results in capacitance change.

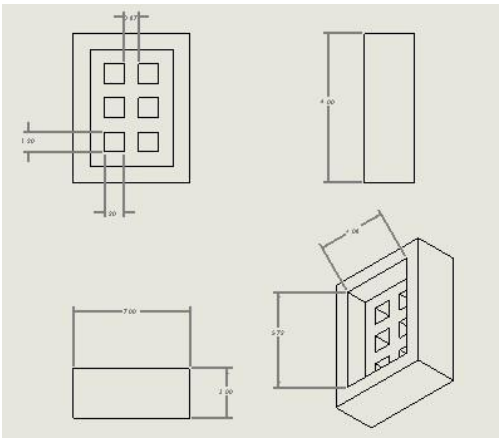

Figure 32. Dimensions of the dielectric mold

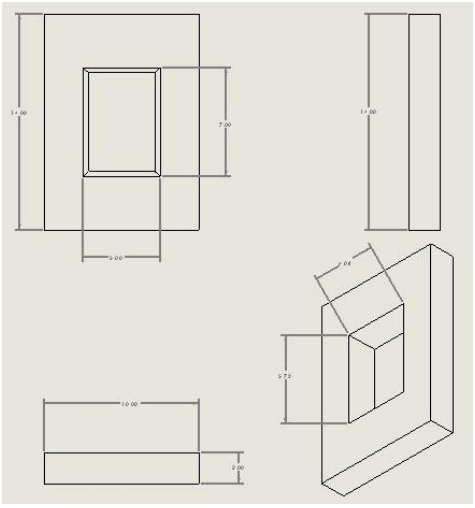

Figure 33. Dimensions of the hard elastomer mold

ii. To establish the dielectric layer between the upper and lower electrodes, a soft elastomer material was employed. The elastomer had dimensions of 5mm by 7mm, with a thickness of 1mm. Additionally, the elastomer

featured 1.26mm square fringes, strategically incorporated to facilitate the measurement of shear forces. These fringes played a crucial role in enhancing the sensor's ability to accurately capture shear force data.

The sensor possesses dimensions of 5mm by 7mm by 5mm, consisting of various components that contribute to its overall structure. The dome component accounts for a height of 2mm, while the dielectric layer measures 2.26mm in thickness. The copper tape, used for the electrodes, has a thickness of 0.04mm, and the PET substrate measures 0.08mm in thickness. The image provided below illustrates the dimensions of each sensor component.

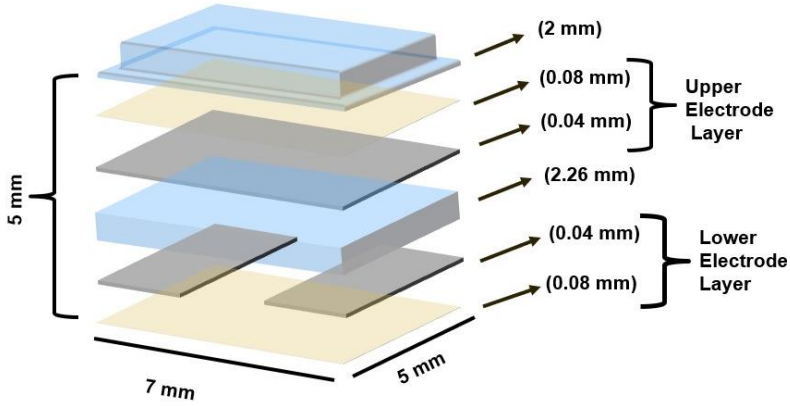


Figure 34. Dimensions of all parts of sensor

To calibrate and test the sensor, the Arduino IDE is employed for interfacing purposes. The experimental setup involved a 3-axis CNC milling machine, which served as a triaxial translation system. The sensor was securely mounted on the CNC machine's bed. For normal and shear forces to act on the sensor, a push-pull force was utilized. The CNC machine's movements were manually controlled using the control panel. The displacement resolution provided by the setup was 10X, equivalent to 1µm. For measuring the applied force, a Digital Force Gauge was employed. The force was incrementally increased from 0N to 10N, with increments of 0.25N.

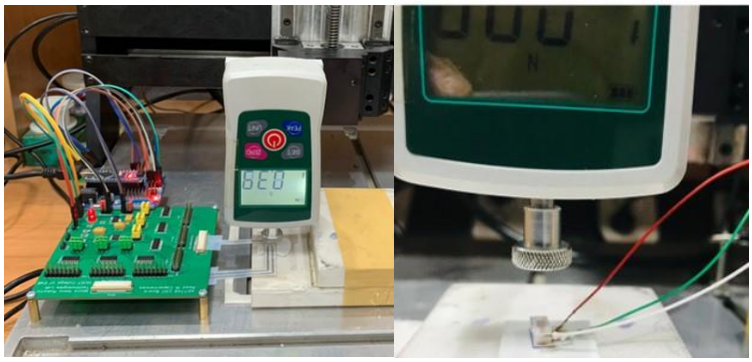

Figure 35. Experimental setup for the characterization of the capacitive tactile sensor

### 3.2.Force Sensitive Resistor (FSR)

Instruments called force sensing resistors (FSR) allow for the measurement of static and/or dynamic forces applied to a surface on which they are placed by altering the resistance of their electric current. Their primary advantages are cheap cost per unit, calibration for human touch applications (forces below 10 kg), little installation space needed (thicknesses under 1.25mm), and a variety of forms and sizes. These sensors are produced by a variety of companies. [2].

Figure 36. Force Sensitive Resistor (FSR) [1]

The output signals from the FSRs must be conditioned to assure precise force readings. To get accurate force data, signal conditioning techniques such as amplification, noise filtering, and calibration are used. For this, analogue circuits or specific microcontrollers can be used. To transform analogue signals into digital ones, this system can use analog-to-digital converters (ADCs). Signal processing algorithms are then applied to the obtained data to extract pertinent force information.

The force feedback system is created using the force data that was collected. To ensure safer and more controlled procedures, haptic wrist band vibrates to notify the surgeon if excessive force is applied during surgery.

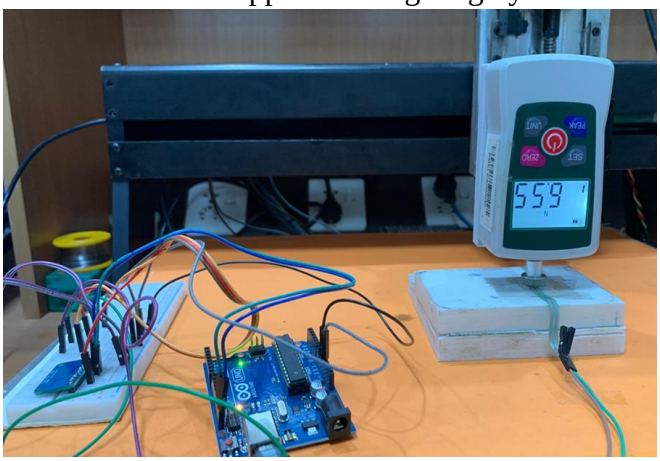

Figure 37. Experimental setup for the characterization of FSR

### 3.3.Actuator

Due to its tiny size and broad frequency range, ERM Vibration Motors were selected to deliver haptic feedback. The mathematical model of the motor is given down below:

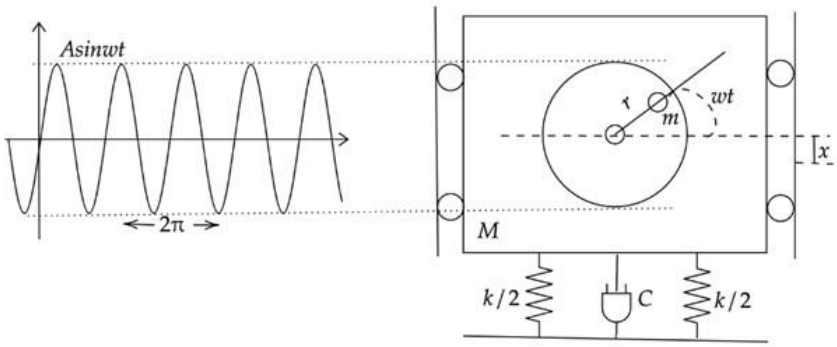


Figure 38. Mass spring damper system representing ERM motor

$x$ is the eccentric mass's displacement in the equations below. Two distinct springs are shown in the diagram, each having a stiffness of $k/2$, displaying an overall stiffness of $k$. It can be regarded as a single spring with stiffness $k$, as defined by Hooke's law.

$$F = kx \tag{3}$$

The mass's velocity is closely correlated with the viscous damping.

$$F = C\frac{dx}{dt} \tag{4}$$

(Velocity is the derivative of displacement).

Newton's second rule of motion governs the mass of the ERM (minus the eccentric mass).

$$F = (M-m)\frac{d^2x}{dt^2} \tag{5}$$

The input $F = F_0 sin(t)$ is equal to the total of these three forces. where $F_0$ is the eccentric mass's centripetal force $F = mr^2$. The eccentric mass's mass is $m$, and the distance from the motor shaft to the eccentric mass's center is $r$. The system's equation of motion may be expressed as:

$$(M-m)\frac{d^2x}{dt^2} + C\frac{dx}{dt} + kx = F_0 sin(\omega t) \tag{6}$$

**Converting into Laplace form:**

$$(M-m)s^2 + Cs + kx = F_0 \frac{w}{w^2+s^2} \quad (7)$$

Where $F0 = mr\omega^2$

$$[(M-m)s2 + Cs + k]X(s) = [F_0 \frac{w}{w^2+s^2}]\, F(s) \quad (8)$$

$$\frac{X(s)}{F(s)} = \frac{(M-m)s^2+Cs+k}{F_0 \frac{w}{w^2+s^2}} \quad (9)$$

Here $M = 1g$ and $m = 0.25g$, $C = 2\ Ns/m$, $k = 8N/m$, $\omega = 2\pi f$ and $r = 5mm$

The similar DC motor circuit that a series-linked DC motor uses to create an ERM is shown below to calculate torque:

The inductance of the windings L is a function of the armature's mechanical design. Because it hinders the reversal of current flow in the armature, it is bad for the motor. Since their smaller mass improves their dynamic performance, coreless or coin motors are less prone to winding inductance. However, pulse-width modulation drive devices may store current via winding inductance.

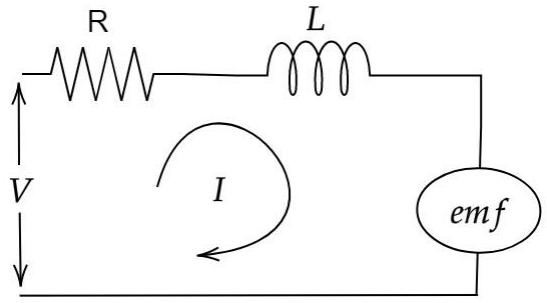


Figure 39. RL equivalent circuit

Most of the motor's losses are brought on by a parasitic component called the resistance to winding R. As the current rises and the motor efficiency falls, the loss from R increases. The Electromotive Force (EMF) is the voltage that develops at the brush terminals when the shaft spins, sometimes known as back EMF. The internal resistance of the EMF is zero. The voltage of the EMF may be given since it is related to the shaft speed:

$$EMF = KE\omega \quad (10)$$

In the equation for the corresponding circuit in steady state, we can plainly observe the linear connection between speed and voltage:

$$V = RI + EMF = RI + KE\omega \quad (11)$$

The current in the circuit of a permanent magnet DC motor is proportional to the torque of T:

$$I = \frac{T}{KT} \quad (12)$$

$$T = I \times K_T \quad (13)$$

The motors are used along with a motor driver PCB. The components that are used in the driver circuit are:

i. 1N4001 Diode
ii. 0.1µF Capacitor
iii. 1KΩ Resistor
iv. 2N2222 NPN Transistor

The driver circuit will control and vary PWMs of the vibratory motors, as per requirements. A haptic wrist band is used to incorporate the ERM motor which acts as the tactile display. The motors are attached at the central zone of the on both sides (Palm and Back). The motor at the palm side gives the force feedback to the surgeon while the motor on the back side gives the information about the lump, if there is a lump, then the motor vibrates. The microcontroller gives the PWM signal at the base of the transistor whose collector is connected to a 3.3V source and emitter is collected to the motor. This method is used to give direct intensity.

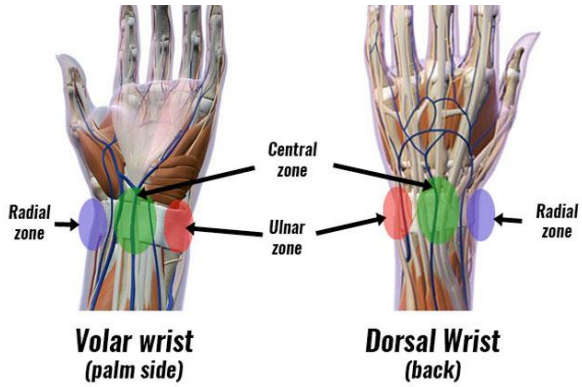


Figure 40. Human Wrist

The intensity of the vibrations depends on the hardness as well as the softness of the material being touched. The ranges of the different hardness and softness are defined. The magnitude of vibration increases as the hardness of the material does. And whenever there is a lump, the other motor will vibrate to indicate that there is a presence of lump.

# CHAPTER 4- HARDWARE

This chapter elaborates on hardware developed which has its imperative role in the project's deliverables. The output of this project is focused on physical implementation hence to achieve project completion, with desired results, requires a working hardware producing appropriate results.

## 4.1.Sensor

Our design incorporates a sensor that operates based on the capacitance change principle. The sensor comprises two conductive plates separated by a dielectric material. Under normal circumstances, without any external force, the capacitance between the plates remains constant. The dielectric layer of the sensor experiences compression when a normal force is applied, reducing the space between the plates. The capacitance of each differential capacitor in the sensor unit cell increases because of this compression. This motion expands the region where the plates overlap, which raises the differential capacitances in that direction [45]. We can precisely calculate the force or pressure acting on the sensor by detecting and examining the capacitance changes. The change in capacitance is inversely proportional to the applied pressure or force.

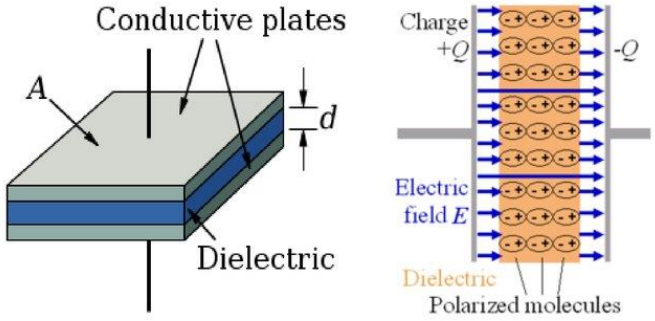


Figure 41. Principle of Capacitance change [48]

The change in capacitance is given by:

$$\Delta C = \frac{\epsilon_o \epsilon_r a}{d}\left(\delta_x + \delta_y + \frac{\delta_x \delta_y}{a}\right) \quad (14)$$

The main components used in the sensor fabricated by us are:

i. Copper Tape
ii. PET Substrate
iii. Eco-Flex 00-30
iv. RTV- 528

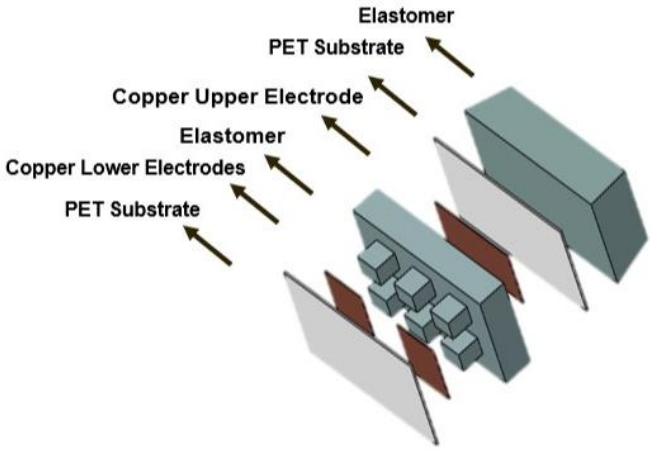


Figure 42. Sensor components with material

### 4.1.1. Working Principle of Sensor

The sensor works by monitoring changes in the differential capacitances between a unit cell structure's four bottom electrodes and center top electrode. This operating principle enables the sensor to effectively capture and measure different types of forces, providing valuable data for various applications.

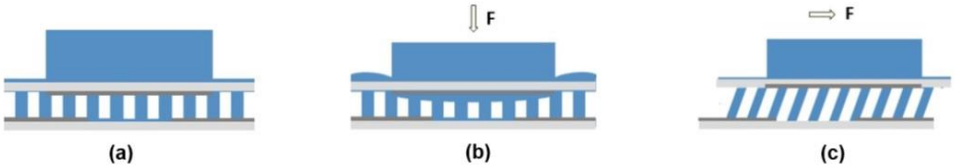


Figure 43. (a) Sensor in normal position. (b) Normal force acting on sensor. (c) Shear force acting on sensor

The fluctuations in the differential capacitances between the central top electrode and the two bottom electrodes are the basis for the change in capacitance in our sensor design. The dielectric layer contracts when an external force, such as a normal force, is applied. This compression results in a reduction of the distance between the plates, leading to an increase in capacitance across all the differential capacitors uniformly. This movement causes an increase in the overlap area between the plates, consequently leading to an increase in the differential capacitances in that direction. By monitoring and analyzing the changes in these differential capacitances, we can accurately measure and quantify the magnitude of the applied force or pressure. This capacitance-based sensing mechanism allows us to effectively capture and interpret the force or pressure exerted on the sensor, enabling precise and reliable measurements.

### 4.1.2. Copper Foil Conductive Tape

The Copper Foil Conductive Tape has a pressure-sensitive acrylic non-

corrosive and electrically conductive adhesive coating on one side. For simple application, it is provided on a releasable liner. For EMI/RFI shielding applications, this kind of tape is frequently used in the electronics sector. Additionally, it is used for wire wrapping, draining static charges from surfaces, seaming shielded rooms, and making surface contact with non-solderable materials. It adheres smoothly without any special preparations [49].

Table 1. Physical Properties [49]

| *Physical Properties* | *Value Imperial (Metric)* |
|---|---|
| *Color - Visual* | Copper |
| *Adhesive* | Electrically Conductive Acrylic |
| *Backing* | Copper Foil - Flat |
| *Flame Retardant[2]* | Pass |

Table 2. Mechanical Properties [49]

| *Mechanical Properties* | *Value Imperial (Metric)* |
|---|---|
| *Backing Thickness - Nominal* | 1.4 mil (0.036 mm) |
| *Total Thickness[1]* | 2.6 +/- 0.2 mils (0.066 +/- 0.005 mm) |
| *Adhesion to Steel[1] - Minimum* | 25 oz/in (2.7 N/cm) |
| *Breaking Strength[1] - Minimum* | 22 lb/in (39 N/cm) |

Table 3. Electrical Properties [49]

| *Electrical Properties* | *Value Imperial (Metric)* |
|---|---|
| *Electrical Resistance[4] - Maximum* | 0.005 Ω/in$^2$ |
| *Shielding Effectiveness[3] - Average 300 kHz – 2.5 GHz* | 66 dB |

### 4.1.3. Ecoflex 00-30

It Ecoflex is a silicone polymer that features platinum catalysis, offering convenient usability and handling. PET (Polyethylene Terephthalate) is a widely used thermoplastic polymer resin from the polyester family. It is commonly employed in the production of plastics for the liquid and food industry, with approximately 30% of global demand for PET being attributed to bottle manufacturing. PET plastic is composed of polymerized ethylene terephthalate units (C10H8O4). This material exhibits a semi-crystalline structure and can appear transparent, opaque, or white, depending on its specific formulation.

The applications of PET include:

i. Plastic bottles and food packaging: PET is extensively used in the production of bottles and packaging materials for various industries.
ii. Thermal insulation: PET can be utilized as a material for thermal insulation due to its insulating properties.
iii. Carrier or backing for magnetic tapes or pressure-sensitive adhesive tapes: PET sheets can serve as a substrate for magnetic tapes or adhesive tapes.

It Ecoflex is a silicone polymer that features platinum catalysis, offering convenient usability and handling. It is composed of two components, referred to as A and B, which are combined in equal parts, both by weight and volume, with a ratio of 1:1. This property ensures that Ecoflex can be easily poured and applied to various molds or surfaces.

Table 4. Characteristic of Eco-flex 00-30 [50]

| | |
|---|---|
| Mix Ratio by Volume | 1A:1B |
| Mix Ratio by Weight | 1A:1B |
| Pot Life | 45 minutes |
| Cure Time | 4 hours |
| Shore Hardness | 00-30 |
| Specific Gravity | 1.07 g/cc |
| Specific Volume | 26.0 cu. in./lb. |
| Tensile Strength | 200 psi |
| 100% Modulus | 10 psi |
| Elongation at Break | 900 % |
| Die B Tear Strength | 38 pli |
| Colour | Translucent |
| Useful Temperature (min) | -65 °F |
| Useful Temperature (max) | 450 °F |
| Shrinkage | <.001 in. / in. |
| Mixed Viscosity | 3,000 cps |

Eco Flex is used to create the dielectric elastomer of the sensor which is placed between electrodes. The change in the dimensions of the elastomer by applying a given force on it changes the displacement.

### 4.1.4. RTV-528 Silicon Rubber

RTV (Room-Temperature Vulcanizing) silicones are a type of silicone that undergoes curing at room temperature without the need for additional heat or specialized curing processes. These silicones are typically formulated using silicone polymers, fillers, and organ reactive silane catalysts. The basic structure of silicone consists of a Si-O bond

with various side chains, providing versatility in its properties. Once applied or molded, RTV silicones exhibit the following features:

i. Good flowability and low viscosity: RTV silicones have a fluid consistency that allows for easy.
ii. Minimal shrinkage: These silicones demonstrate minimal shrinkage during the curing process, ensuring dimensional stability and accurate replication of the original shape.
iii. Optimal tension: RTV silicones offer excellent tensile strength, allowing them to withstand mechanical stress and deformation.
iv. Distortion resistance: Once cured, RTV silicones maintain their shape without experiencing distortion or warping.
v. Favorable hardness: RTV silicones can be formulated to exhibit a range of hardness levels.
vi. Age resistance, acid and alkali resistance, and high temperature resistance: RTV silicones possess excellent thermal stability, along with resistance to chemical substances like acids, alkalis, and aging factors.

### 4.2.FSR 400 Sensor

It is a durable polymer thick film (PTF) device that shows resistance decreasing when more force is applied to the sensor's surface. A force-sensing resistor (FSR) with the FSR400 is made specifically to measure and identify applied force or pressure. It is appropriate for a variety of applications thanks to its strong and compact design [46]. It is the smallest commercially available force sensor.

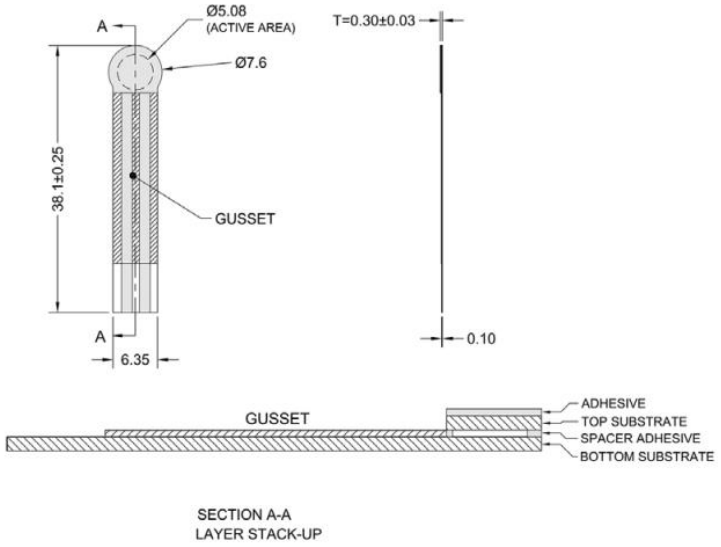


Figure 44. Sensor dimensions and mechanical data [46]

The following are the sensor's primary components: The resistive substance used

in the FSR400 changes resistance in response to force or pressure.

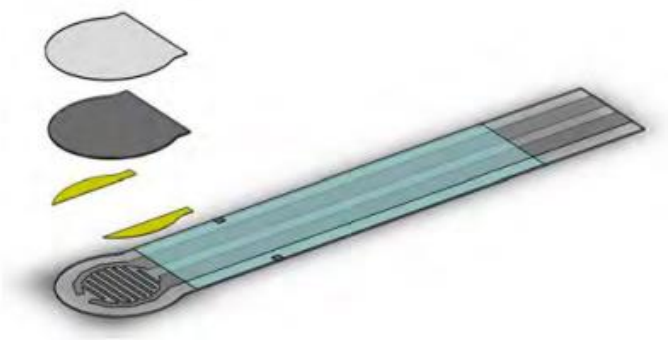

Figure 45. Exploded view of FSR [46]

Two electrodes that are in direct touch with the sensing element are included in the FSR400. To transfer force through the sensor, the sensing element must be positioned between the electrodes.

Table 5. Specifications of Fsr400 [46]

| | |
|---|---|
| Actuation Force | ~0.2N min |
| Force Sensitivity Range* | ~0.2N – 20N |
| Force Resolution | Continuous (analog) |
| Force Repeatability Single Part | +/- 2% |
| Force Repeatability Part to Part | +/- 6% (Single Batch) |
| Non-Actuated Resistance | >10 MΩ |
| Hysteresis | +10% Average (RF+ - RF-)/RF+ |
| Device Rise Time | < 3 Microseconds |

### 4.3.Angular Position Encoder

The sensor employed in our design for forceps angle measurement is AS5600 12-bit programmable contactless potentiometer magnetic position encoder based on Hall Effect principle. Hall effect sensors produce a voltage known as Hall voltage when they detect the existence and strength of the magnetic field within their range. [55]. This hall voltage is then amplified and sent to the internal 12-bit ADC for digitalization. After that the data can be obtained in the microcontroller using $I^2C$ protocol for serial communication using SCL and SDA pins using the slave address 0x36 or analog data (processed through a 12-bit DAC) can be obtained from OUT pin [56].

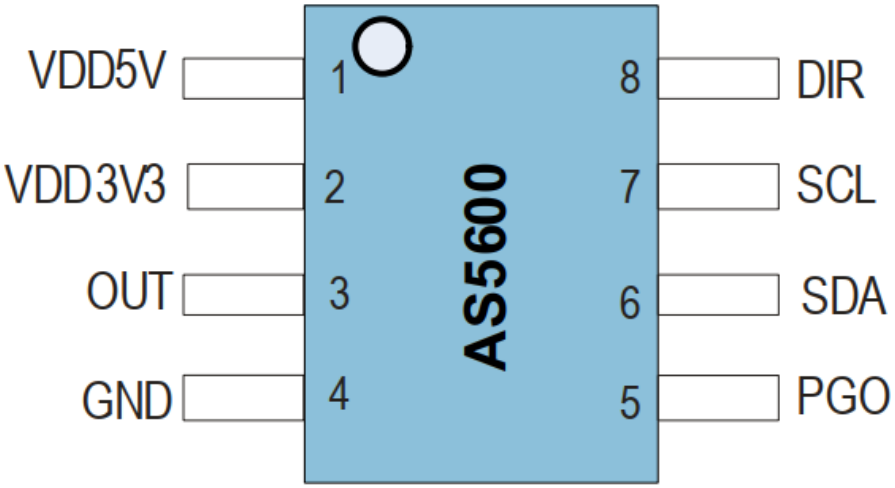


Figure 46. Position Encoder Chip [56]

The pin description of this encoder IC is shown in the table:

Table 6. Pinout Description of AS5600 Encoder [56]

| Pin Number | Name | Type | Description |
|---|---|---|---|
| 1 | VDD5V | Supply | Positive voltage supply in 5V mode (requires 100nF decoupling capacitor) |
| 2 | VDD3V3 | Supply | Positive voltage supply in 3.3V mode (requires an external 1-µF decoupling capacitor in 5V mode) |
| 3 | OUT | Analog/digital output | Analog/PWM output |
| 4 | GND | Supply | Ground |
| 5 | PGO | Digital input | Program option (internal pull-up, connected to GND = Programming Option B) |
| 6 | SDA | Digital input/output | I²C Data (consider external pull-up) |
| 7 | SCL | Digital input | I²C Clock (consider external pull-up) |
| 8 | DIR | Digital input | Direction polarity (GND = values increase clockwise, VDD = values increase counterclockwise) |

### 4.3.1. Working Principle of Sensor

When the magnetic field on the hall sensor, the data from the hall element is processed through the ADC and after that an advanced algorithm Coordinate Rotation Digital Computer (CORDIC) is applied to measure the strength and orientation of the magnetic field and based on that detect quadrant and position angle of the magnet. The resulting digital value can be directly read through $I^2C$ protocol, or it can be further processed through DAC to obtain an analog output.

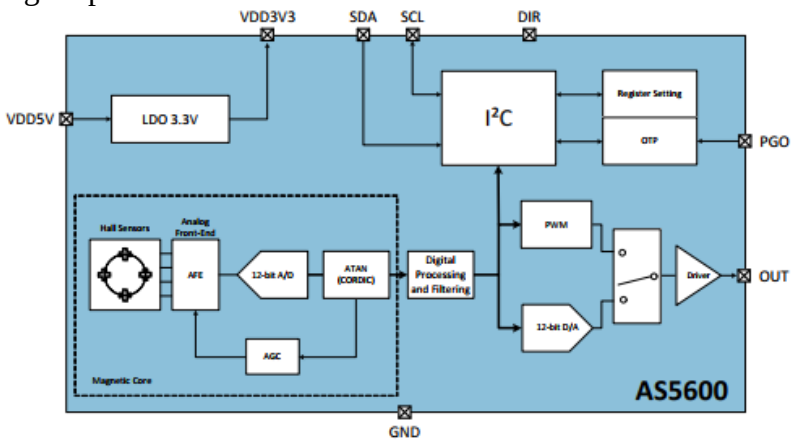


Figure 47. Block diagram of Encoder IC [56]

### 4.3.2. Measuring Setup and Sensitivity

The measuring setup for the sensor is composed of a diametrically magnetized neodymium magnet placed parallel to the chip at ~0.5mm to ~3mm spacing [56].

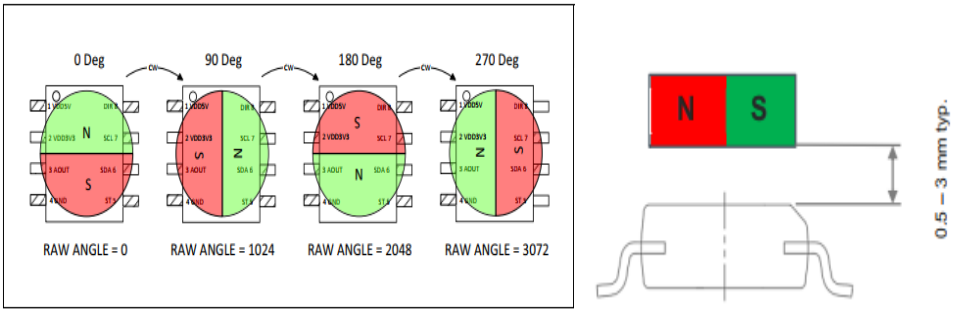


(a) (b)

Figure 48. (a) Setup diagram for measuring angular position [56]
(b) Airgap (spacing) for optimal operation [56]

The 12-bit DAC enables this IC to record 4096 instances during one rotation [56] which ultimately means that the sensitivity of the encoder can be found as:

$$Sensitivity = \frac{360^\circ}{4096} \approx 0.0879^\circ$$

This encoder is highly repeatable and sensitive which makes it an ideal

choice for the sensitive applications such as forceps angle during surgical procedures.

### 4.3.3. Power Ratings

One of the outstanding operational advantages of this encoder is its automatic Low Power Mode (LPM) initialization, that is when there is no change in magnetic field after a certain time period the IC goes into low power mode consuming less than usual power. The maximum ratings of the encoder are given below.

Table 7. Voltage and Power ratings for AS5600 Encoder [56]

| Symbol | Parameter | Min | Max | Units | Comments |
|---|---|---|---|---|---|
| **Electrical Parameters** | | | | | |
| VDD5V | DC Supply Voltage at VDD5V pin | -0.3 | 6.1 | V | |
| VDD3V3 | DC Supply Voltage at VDD3V3 pin | -0.3 | 4.0 | V | |
| VIO | DC Supply Voltage at all digital or analog pins | -0.3 | VDD+0.3 | V | |
| $I_{SCR}$ | Input current (latch-up immunity) | -100 | 100 | mA | JESD78 |
| **Continuous Power Dissipation ($T_A$ = 70°C)** | | | | | |
| $P_T$ | Continuous power dissipation | | 50 | mW | |

Low power mode, power consumption ratings are shown in the table below:

Table 8. LPM Power Consumption Ratings [56]

| Symbol | Parameter | Conditions | Min | Typ | Max | Units |
|---|---|---|---|---|---|---|
| VDD5V | Positive supply voltage in 5.0V mode | 5.0V operation mode | 4.5 | 5.0 | 5.5 | V |
| | | During OTP burn procedure (2) | | | | |
| VDD3V3 | Positive supply voltage in 3.3V mode | 3.3V operation mode | 3.0 | 3.3 | 3.6 | V |
| | | During OTP burn procedure (2) | 3.25 | 3.3 | 3.35 | V |
| IDD | Supply current in NOM (1) | PM = 00<br>Always on | | | 6.5 | mA |
| IDD_LPM1 | Supply current in LPM1 (1) | PM = 01<br>Polling time = 5ms | | | 3.4 | mA |
| IDD_ LPM2 | Supply current in LPM2 (1) | PM = 10<br>Polling time = 20ms | | | 1.8 | mA |
| IDD_ LPM3 | Supply current in LPM3 (1) | PM = 11<br>Polling time = 100ms | | | 1.5 | mA |

### 4.4.ADS1115 16-Bit ADC

The ADS1115 is a 16-bit, delta-Sigma (Δ-∑) external ADC chip that incorporates hardware design to measure the resistive force through a force sensing resistor (FSR). FSR changes its resistance based on force application on it and through voltage divider circuit and based on resistance voltage across the FSR is measured through ADC. The pinout of the IC chip is shown below:

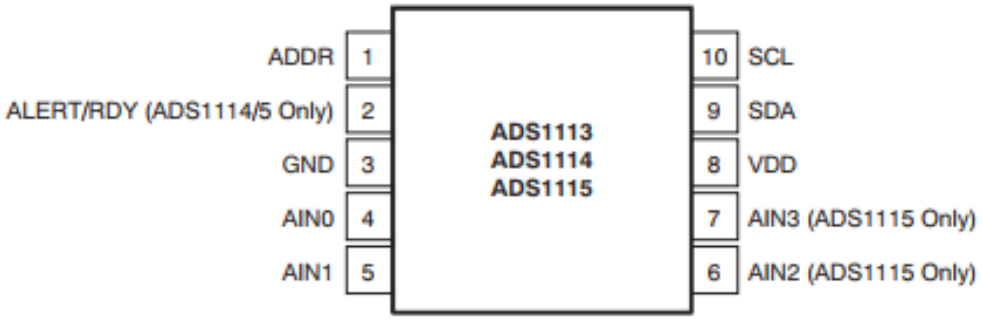


Figure 49.ADS1115 IC chip [57]

The pin description of this ADC is shown in the table:

Table 9. Pinout Description of ADS1115 [57]

| PIN # | DEVICE | | | ANALOG/ DIGITAL INPUT/ OUTPUT | DESCRIPTION |
|---|---|---|---|---|---|
| | ADS1113 | ADS1114 | ADS1115 | | |
| 1 | ADDR | ADDR | ADDR | Digital Input | I²C slave address select |
| 2 | NC (1) | ALERT/RDY | ALERT/RDY | Digital Output | Digital comparator output or conversion ready (NC for ADS1113) |
| 3 | GND | GND | GND | Analog | Ground |
| 4 | AIN0 | AIN0 | AIN0 | Analog Input | Differential channel 1: Positive input or single-ended channel 1 input |
| 5 | AIN1 | AIN1 | AIN1 | Analog Input | Differential channel 1: Negative input or single-ended channel 2 input |
| 6 | NC | NC | AIN2 | Analog Input | Differential channel 2: Positive input or single-ended channel 3 input (NC for ADS1113/4) |
| 7 | NC | NC | AIN3 | Analog Input | Differential channel 2: Negative input or single-ended channel 4 input (NC for ADS1113/4) |
| 8 | VDD | VDD | VDD | Analog | Power supply: 2.0V to 5.5V |
| 9 | SDA | SDA | SDA | Digital I/O | Serial data: Transmits and receives data |
| 10 | SCL | SCL | SCL | Digital Input | Serial clock input: Clocks data on SDA |

#### 4.4.1. Maximum Power ratings

ADS1115 is a low power consumption ADC, and its high resolution and small size makes it one of the best low-cost ADCs available in the market. The maximum power ratings of the ADC are shown below:

Table 10. Maximum Power Ratings for ADS1115 [57]

| | ADS1113, ADS1114, ADS1115 | UNIT |
|---|---|---|
| VDD to GND | –0.3 to +5.5 | V |
| Analog input current | 100, momentary | mA |
| Analog input current | 10, continuous | mA |
| Analog input voltage to GND | –0.3 to VDD + 0.3 | V |
| SDA, SCL, ADDR, ALERT/RDY voltage to GND | –0.5 to +5.5 | V |
| Maximum junction temperature | +150 | °C |
| Operating temperature range | –40 to +140 | °C |
| Storage temperature range | –60 to +150 | °C |

### 4.4.2. Working Principle of ADS1115

The ADC works on delta-Sigma principle, basic setting of sigma delta configuration consists of an integrator, a summation operator, a comparator and a 1-bit DAC are used. The summer accumulates the charge and integrator integrates the new value with the previously stored data and then after comparison in the comparator with the reference voltage, the comparator sends back a 1-bit data through the DAC to the summer and the next iteration is performed.

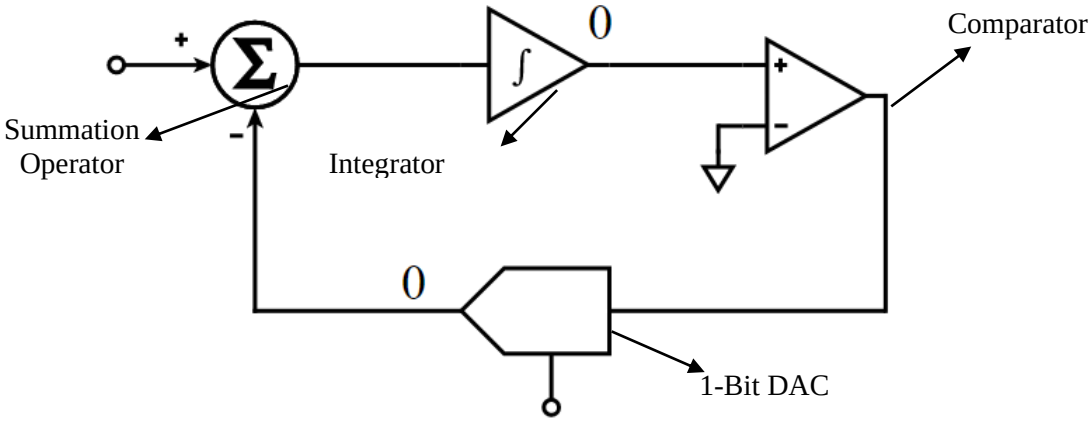


Figure 50. Delta-Sigma working [58]

The data after being processed through Δ-∑ modulator then pass through a fourth order low-pass filter that attenuates any noise in the signal after that the signal is transmitted to the microcontroller using serial communication i.e. $I^2C$.

### 4.4.3. Gain and Reference voltage selection

The ADS1115 provides the facility to optimize the sampled data by providing different gain selections through a Programmable Gain Amplifier (PGA) implemented before Δ-∑ modulator. The table below shows different full-scale ranges.

Table 11. Full Scale Ranges and Resolution of ADS1115 for Different Amplifier Gains [57]

| PGA Setting | Full-Scale range (V) | Resolution (mV) |
|---|---|---|
| Two-thirds | ±6.144 | 0.1875 |
| One | ±4.096 | 0.125 |
| Two | ±2.0448 | 0.0625 |
| Four | ±1.024 | 0.03125 |
| Eight | ±0.512 | 0.015625 |
| Sixteen | ±0.256 | 0.0078125 |

### 4.4.4. Aliasing prevention

When the frequency of input data contains frequencies that are higher than half of the data rate aliasing occurs which is the overlapping of data samples, this phenomenon tends to distort the input signal and the output becomes

faulty. To prevent aliasing, an anti-aliasing attenuator is applied in the form of an RC filter before sampling, it attenuates any high frequency noise from the signal and provides adequately correct output response. Figure 50 shows a simple Anti-Aliasing Filter (AAF).

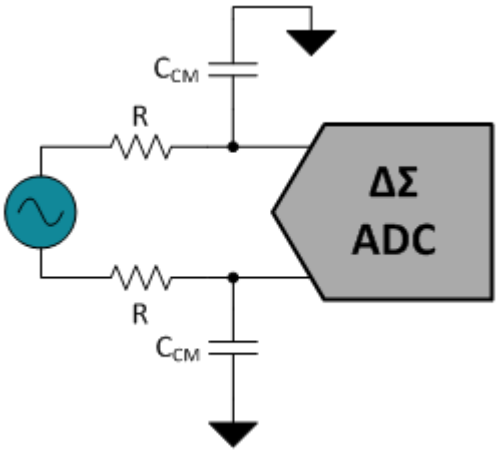


Figure 51. A Simple Anti-Aliasing filter to prevent aliasing in the input data [59]

### 4.4.5. Serial Data Communication I²C

After the signal processing when the data is ready it can be received in the microcontroller for further processing. The I²C bus is used to communicate devices with the microcontroller. The I²C interface of the ADS1115 is quite effective and accommodating, it provides an ADDR pin to configure the address to prevent same address for multiple devices which cannot work on the I²C. The default address of the ADC is 0x48, but in case there is another device that has the same address i.e., 0x48, the address of the ADC can be configured by connecting it to certain pins of the ADC IC [57]. The detail of the configuration is shared in table 12.

Table 12. ADDR Pin Connection Configuration and Corresponding Slave Addresses [57]

| ADDR Pin Connection | ADC I²C Address |
|---|---|
| GND | 0x48 (default) |
| VDD | 0x49 |
| SDA | 0x4A |
| SCL | 0x4B |

## 4.5.AD7746 24-Bit Capacitance to Digital Converter (CDC)

A high-resolution Capacitance to Digital converter is the AD7746. that allows capacitance readings with an accuracy of 4fF ($4 \times 10^{-15} F$). It has a built-in temperature sensor with a resolution of 0.1°C and accuracy of +/- 2°C to prevent accidental burnouts and other electronic failures such as short-circuit etc. [6]

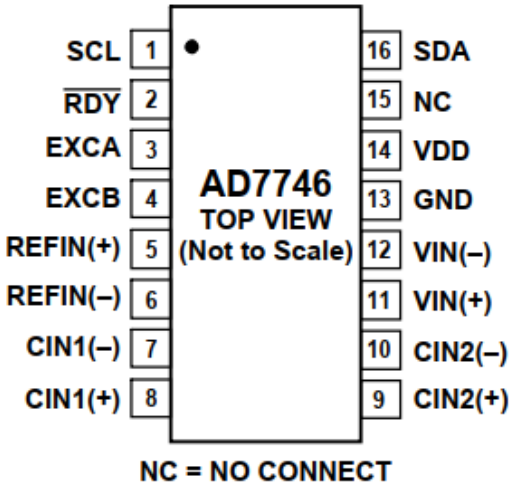


Figure 52. Pin configuration of AD7746 CDC [60]

The pin description of this CDC is shown in the table:

Table 13. Pin Description of AD7746 CDC [60]

| Pin No. | Mnemonic | Description |
|---|---|---|
| 1 | SCL | Serial Interface Clock Input. Connects to the master clock line. Requires pull-up resistor if not already provided in the system. |
| 2 | $\overline{\text{RDY}}$ | Logic Output. A falling edge on this output indicates that a conversion on enabled channel(s) has been finished and the new data is available. Alternatively, the status register can be read via the 2-wire serial interface and the relevant bit(s) decoded to query the finished conversion. If not used, this pin should be left as an open circuit. |
| 3, 4 | EXCA, EXCB | CDC Excitation Outputs. The measured capacitance is connected between one of the EXC pins and one of the CIN pins. If not used, these pins should be left as an open circuit. |
| 5, 6 | REFIN(+), REFIN(–) | Differential Voltage Reference Input for the Voltage Channel (ADC). Alternatively, the on-chip internal reference can be used for the voltage channel. These reference input pins are not used for conversion on capacitive channel(s) (CDC). If not used, these pins can be left as an open circuit or connected to GND. |
| 7 | CIN1(–) | CDC Negative Capacitive Input in Differential Mode. This pin is internally disconnected in single-ended CDC configuration. If not used, this pin can be left as an open circuit or connected to GND. |
| 8 | CIN1(+) | CDC Capacitive Input (in Single-Ended Mode) or Positive Capacitive Input (in Differential Mode). The measured capacitance is connected between one of the EXC pins and one of the CIN pins. If not used, this pin can be left as an open circuit or connected to GND. |
| 9, 10 (AD7745) | NC | Not Connected. This pin should be left as an open circuit. |
| 9 (AD7746) | CIN2(+) | CDC Second Capacitive Input (in Single-Ended Mode) or Positive Capacitive Input (in Differential Mode). If not used, this pin can be left open circuit or connected to GND. |
| 10 (AD7746) | CIN2(–) | CDC Negative Capacitive Input in Differential Mode. This pin is internally disconnected in a single-ended CDC configuration. If not used, this pin can be left as an open circuit or connected to GND. |
| 11, 12 | VIN(+), VIN(–) | Differential Voltage Input for the Voltage Channel (ADC). These pins are also used to connect an external temperature sensing diode. If not used, these pins can be left as an open circuit or connected to GND. |
| 13 | GND | Ground Pin. |
| 14 | VDD | Power Supply Voltage. This pin should be decoupled to GND, using a low impedance capacitor, for example in combination with a 10 µF tantalum and a 0.1 µF multilayer ceramic. |
| 15 | NC | Not Connected. This pin should be left as an open circuit. |
| 16 | SDA | Serial Interface Bidirectional Data. Connects to the master data line. Requires a pull-up resistor if not provided elsewhere in the system. |

### 4.5.1. Maximum Power ratings

AD7746 is a low power (0.7mA current consumption) CDC [60], and its high resolution and small size makes it one of the best CDCs available in the market. The maximum power ratings of the ADC are shown below:

Table 14. Absolute Maximum Ratings for Optimal Operation of AD7746 [60]

| Parameter | Rating |
|---|---|
| Positive Supply Voltage $V_{DD}$ to GND | –0.3 V to +6.5 V |
| Voltage on any Input or Output Pin to GND | –0.3 V to $V_{DD}$ + 0.3 V |
| ESD Rating (ESD Association Human Body Model, S5.1) | 2000 V |
| Operating Temperature Range | –40°C to +125°C |
| Storage Temperature Range | –65°C to +150°C |
| Junction Temperature | 150°C |
| TSSOP Package $\theta_{JA}$, (Thermal Impedance-to-Air) | 128°C/W |
| TSSOP Package $\theta_{JC}$, (Thermal Impedance-to-Case) | 14°C/W |
| Lead Temperature, Soldering | |
| Vapor Phase (60 sec) | 215°C |
| Infrared (15 sec) | 220°C |

### 4.5.2. Working Principle of AD7746

AD7746 works on the similar principle of Δ-∑ modulation but with a higher resolution (24-bit) than that of ADS1115 (16-bit). The block diagram of the internal working of CDC is shown. The capacitance data from the respective channel (selected by the multiplexer) is fed to the modulator for conversion and after that it is passed through a digital filter and after that it can be monitored or further processed by accessing it through $I^2C$ protocol slave address 0x48 [60].

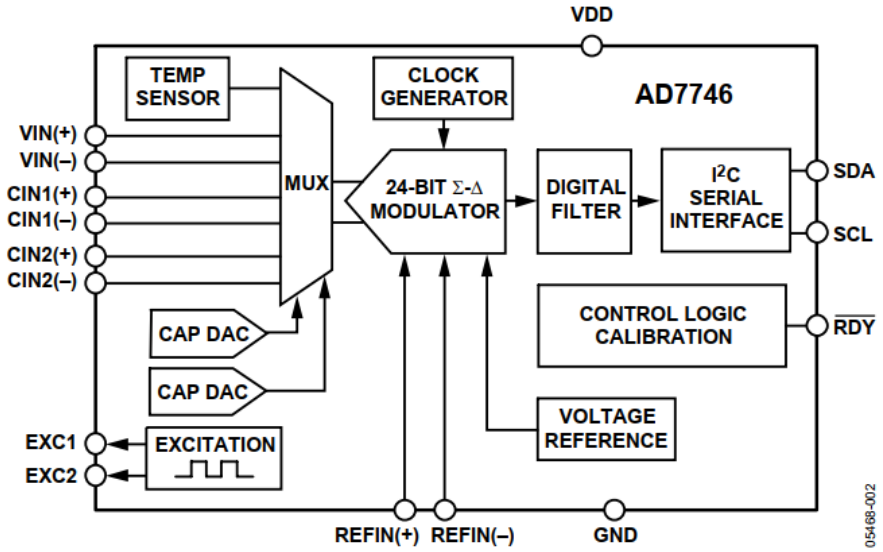


Figure 53. Block diagram of AD7746 working [60]

## 4.6.Microcontroller (ESP32-WROOM-32)

ESP32-WROOM-32 is one of the best available low-cost low power

consumption microcontrollers universally available with exceptionally high relative performance along with wireless communication through 2.4 GHz Wi-Fi module and Bluetooth module V4.2 for small-distance communications. ESP32 provides a wide range of peripherals that includes Ethernet connection, $I^2C$, SPI, UART, I2S and SD card interface communication protocols. It comes with a 40.0 MHz built-in crystal making it a high-speed controller adequate for sensitive applications such as RF communications and data transmission [53].

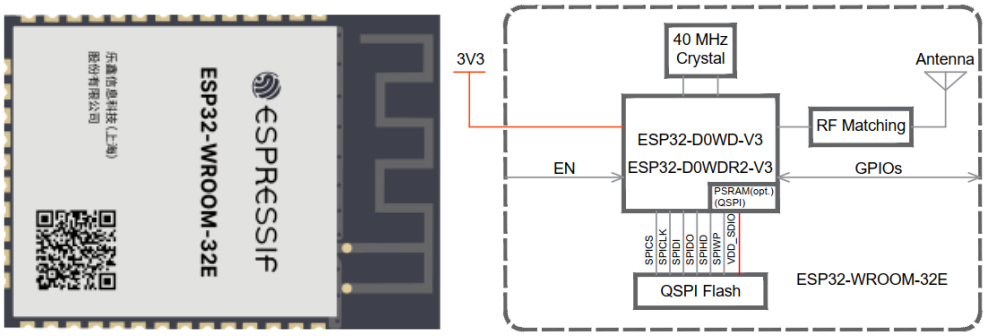


(a) (b)

Figure 54. ESP32-WROOM-32E microcontroller (a) ESP32 Module (b) Block Diagram [53]

The pin description of ESP32 is shown:

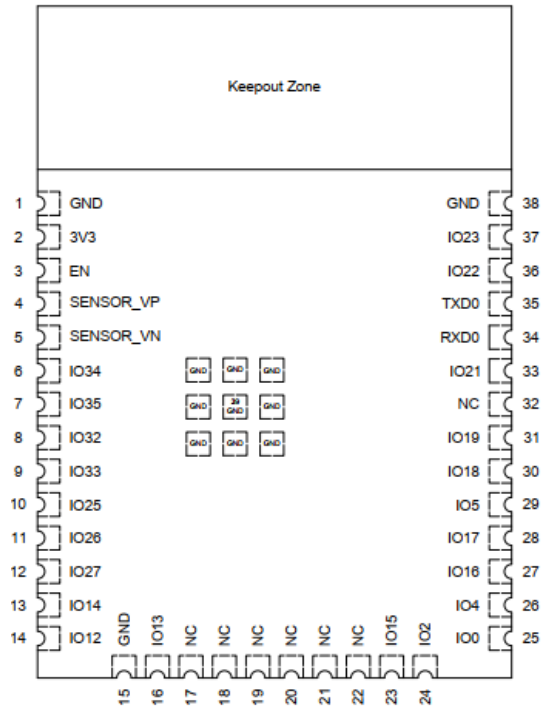


Figure 55. ESP32WROOM -32 pinout[53]

### 4.6.1. $I^2C$ Communication protocol

ESP32 provides the flexibility to configure any of the general-purpose input output pins (GPIOs) as $I^2C$ bus channels, but default pins that are used for

this communication are GPIO22 (SCL) and GPIO21 (SDA). In this type of communication usually microcontroller is the Master device such as in our project ESP32 is the master device communicating with three slave devices namely AS5600, ADS1115 and AD7746. The master device generates the clock. All the other devices will remain "silent" unless their address is on the data line when the acknowledgment bit is transmitted. After successful transmission of data, the communication stops when data line (SDA) goes from low logic to high logic while clock pulse (SCL) is high [61]. A typical setup of $I^2C$ communication is shown below.

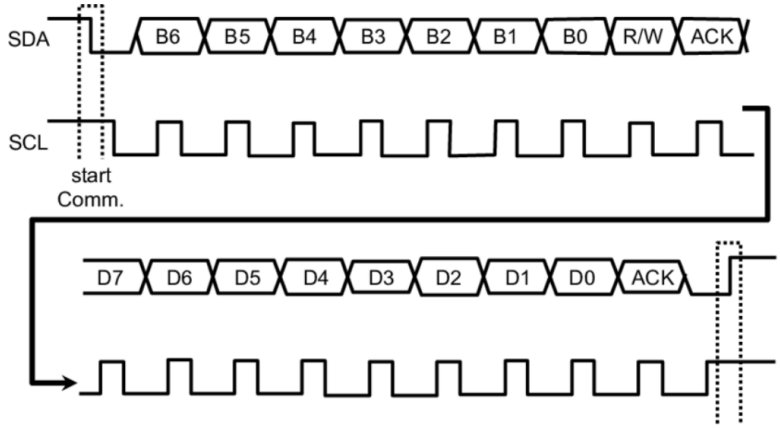


Figure 56. I2C communication protocol timing diagram [61]

### 4.6.2. ESP32 Programming Protocol

ESP32 is programmed using a USB to TTL converter IC i.e., FTDI-RS232. This converter IC converts the USB data (program) into TTL logic that is compatible with the microcontroller and let us program these devices easily, normally ESP32- development boards do have an FTDI converter, and a USB port mounted on it, but we decided to not use the development board and instead use the smaller sized chip and program it through standalone FTDI converter. The figure below shows the FTDI converter used to program the ESP32.


Figure 57. FTDI-RS232 USB to TTL converter [62]

### 4.6.3. ESP32 Power Ratings

ESP32 is a low power consumption that can automatically adjust between power options as needed by the application some of the power levels during RF communication mode are shown in the table.

Table 15. Esp32 Current Consumption Ratings During Rf Modes [53]

| Work mode | Description | | Average (mA) | Peak (mA) |
|---|---|---|---|---|
| Active (RF working) | TX | 802.11b, 20 MHz, 1 Mbps, @19.5 dBm | 239 | 379 |
| | | 802.11g, 20 MHz, 54 Mbps, @15 dBm | 190 | 276 |
| | | 802.11n, 20 MHz, MCS7, @13 dBm | 183 | 258 |
| | | 802.11n, 40 MHz, MCS7, @13 dBm | 165 | 211 |
| | RX | 802.11b/g/n, 20 MHz | 112 | 112 |
| | | 802.11n, 40 MHz | 118 | 118 |

## 4.7.ERM Motors

Eccentric rotating mass vibration (ERM) motors are also known as coreless dc motors or brushless dc motors. Its foundation is a conventional DC motor with an imbalanced mass connected to the shaft. Different vibration frequencies and intensities are created by spinning the offset mass at various speeds. The ERM is connected to it and used to vibrate the final device.

There are two different formats for ERMs. The most common shape is a bar, while a coin form is also available for more portable solutions. Although the two solutions share the same principles, they are constructed in very different ways.

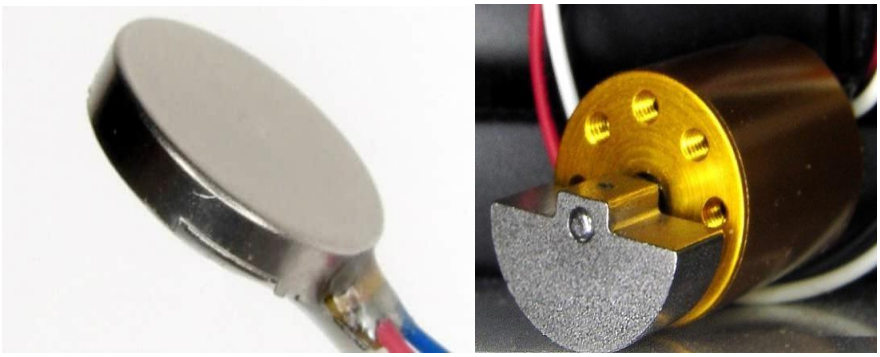

(a) (b)

Figure 58. ERM vibration motors, (a) Coin type, (b) Cylinder type

When comparing an ERM solution to other actuator systems, there are a few factors that are especially important to consider. DC voltage is used as an ERM's input. As the input voltage increases, the vibration intensity typically increases as well.

### 4.7.1. Principle of ERM Motors

Pager motors, also known as eccentric rotating mass vibration motors, are DC motors with an offset (non-symmetric) mass attached to the shaft. As the ERM turns, the offset mass's centripetal force is out of balance, producing a net centrifugal force that starts the motor moving. Due to the enormous number of revolutions per minute, these asymmetric forces push and continuously move the motor. The outcome of this repeated movement is a vibration.

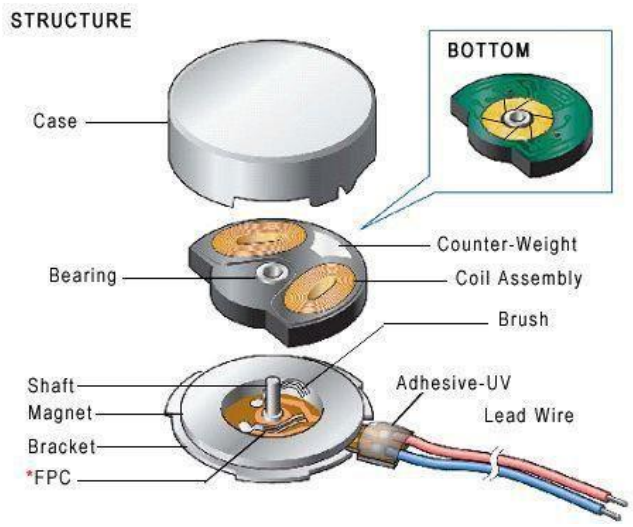


Figure 59 Structure of a coin ERM motor

The DC motor, which in some way spins the mass, is in working order. A simple DC motor can be created using a battery, two magnets with opposite poles, and a single coil of wire. They exert the highest force when they are perpendicular.

When the coil is in the vertical position, it is severed. As a result, there is no current or force, but it still spins because of inertia. After crossing vertically, the coil's sides are flipped, but the force continues to act in the same direction. A genuine DC motor features multiple coil windings to maximize torque.

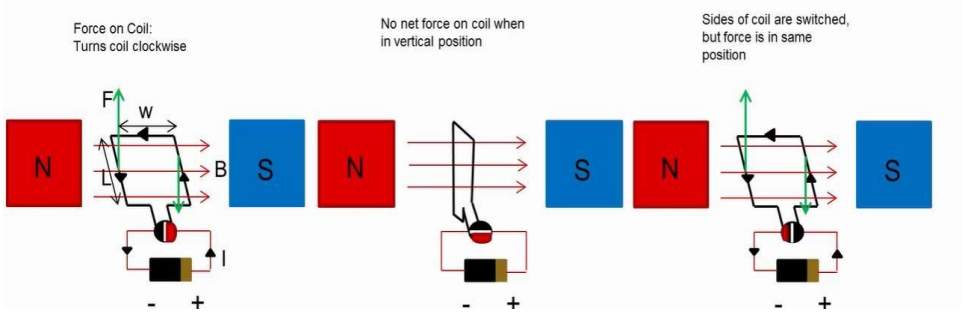


Figure 60 Working of a DC motor

As more evenly spaced coils are added, the net force on all the coils becomes independent of the angle and can be thought of as a constant proportional to the input current. As the coil spins in the magnetic field, a back EMF is produced that, in accordance with Faraday's equation, is proportional to the angular velocity.[50]

It's also important to remember that an ERM's rotational velocity and vibration frequency are linked. This directly depends on the input voltage. This suggests that it is impossible to alter the vibrations' amplitude and frequency separately.

Table 16. Features Of Erm Motor [51]

| | |
|---|---|
| Place of Origin | Guangdong, China (Mainland) |
| Model Number | LCM-0820 |
| Usage | Mobile phone, Watch and Band, Massagers, Medical apparatus and instruments |
| Certification | ISO9001, ISO14001, OHSAS18001 |
| Type | Micro Motor |
| Commutation | Brush |
| Feature | Vibration |
| Rated Voltage | 3.0(V) DC |
| Rated speed | 9000rpm Min |
| Rated current | 80 mA Max |
| Starting voltage | 2.3(V) DC |
| Vibration test | 0.4±0.2G |
| Operating voltage | 2.7~3.3(V) DC |
| Life | 2.5S on,2.5S off, 3,000 cycles |

### 4.8.Haptic Motor Driver PCB

The board is designed to control and vary PWM of the motor. The flow diagram of the circuit is shown below:

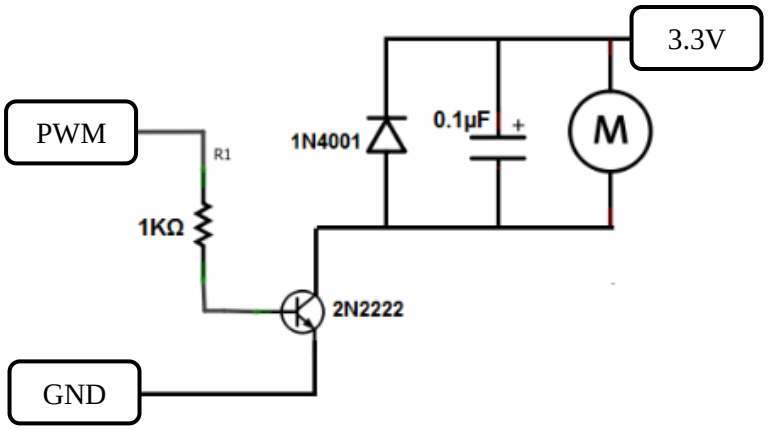


Figure 61. Motor driver board

### 4.8.1. Principle of Motor Driver

It's crucial to connect a diode that is reverse biased in parallel to the motor when using a microcontroller to drive it. This still holds true whether a motor controller or transistor is used to drive it. These voltages quickly kill the microcontroller without the diode. In the straightforward circuit we have above, we only have a voltage source because no diode is required when merely powering the vibration motor directly with DC voltage.

The $0.1\mu$F capacitor smooths down voltage peaks caused by the opening and closing of the brushes, which are contacts that carry current to the motor windings.

Utilization of a transistor (2N2222) since most microcontrollers have weak current outputs, which means that they cannot drive a wide range of electronic devices. A transistor is placed to provide current amplification to compensate for this insufficient current output. The 2N2222 transistor we're utilizing at this place serves this purpose. To run the vibration motor, around 75mA of current is required. We can drive the motor due to the transistor. A 1K resistor in series relates to the transistor base to ensure that an excessive amount of current does not flow from the output. This reduces current to a safe level so that the motor isn't being powered by an excessive quantity. Remember that the base current entering through a transistor is typically amplified by around 100 times. Too much current can harm the motor if there isn't a resistor at the base or the output. The value of the 1KΩ resistor is not exact. Any value up to around 5KΩ can be used.

### 4.9.3D Printed parts

All parts of the tool are 3D printed including the handle, grasper jaws, and outer covering except the internal rod which is made of brass rod. The material used for 3D printing is engineering resin which is also called engineering plastic or engineering polymer that possesses enhanced mechanical and chemical properties. Engineering resins have exceptional strength, stiffness, toughness, heat resistance, chemical resistance, and dimensional stability. Apart from that engineering resin is also biocompatible. Due to such exceptional properties engineering resin is the best fit for the 3D printing of laparoscopic tools.

Table 17. Properties of Engineering Resin

**Mechanical properties**

| | METHOD | DATA |
|---|---|---|
| **Shore Hardness** | ASTM: D2240-05 | 82D |
| **Tensile Strength** | ASTM: D638-14 | 48.5MPa |
| **Flexural Strength** | ASTM: D790-10 | 60.8MPa |
| **Elongation at Break** | ASTM: D638-14 | 16.80% |
| **Viscosity (25℃)** | ASTM: D4212-10 | 365mpa.s |
| **Notched IZOD** | ASTM: D256-10 | 58.4J/m |
| **HDT (0.455MPa)** | ASTM: D648-18 | 60℃ |

Figure 62. Grasper of laparoscopic tool

The material used for the internal rod was brass as it has much higher strength than the engineering resin and is suitable for transferring force from one end to the other effectively.

## 4.10.Mechanism of grasper

The mechanism of grasper was a crucial part of the whole laparoscopic tool which is used to hold tissue inside a patient's body. The force applied to the tissue was to be determined by a sensor integrated into the grasper. For this purpose, a special slot was designed in the gripping jaw of the tool so that sensor values remain accurate, and it does not get in contact with tissue and damage it.

We implemented multiple mechanism designs for our project. Our first design was of double-action grasper. In this mechanism, the force was applied by the internal rod on both jaws of grasper and both jaws were movable.

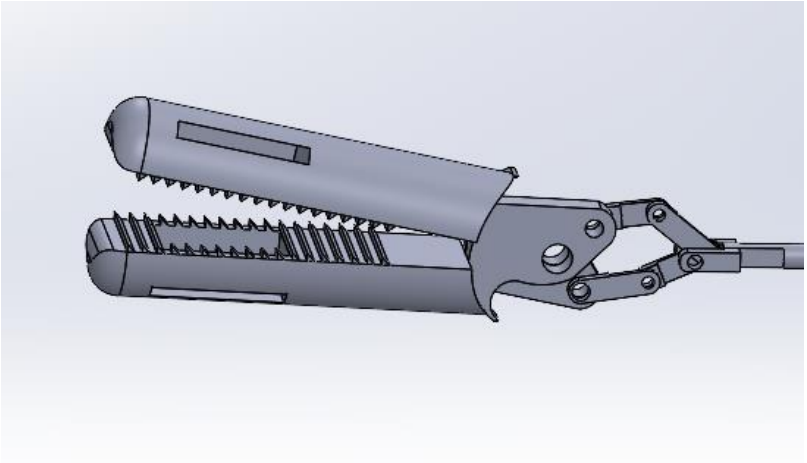

Figure 63. Double action grasper mechanism

Our next design was based on a single action grasper, in which one jaw was movable while the other was static in this type of mechanism our previous problem was solved as the sensor was placed inside the static jaw and the values, we get were much better than before. Apart from the motion issue we also faced some size constraint issues which were resolved in our final jaw mechanism. [54]

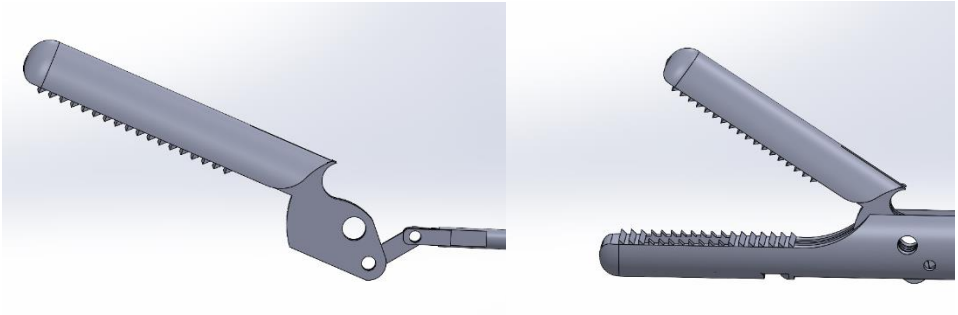

Figure 64. Single action grasper mechanism [54]

This was our final and most accurate jaw mechanism. It was working on a single action jaw mechanism, in which one jaw is static and the other jaw is movable.

## 4.11.Parts of the tool and their functions

Our tool was made of multiple parts some of them are mentioned as follows.

i. Handle
ii. Casing for Electronic circuitry
iii. Internal rod
iv. Covering over the internal rod
v. Grasper jaws (upper and lower)

### 4.11.1. Handle

The main component of our tool was the handle which was used to hold the tool. It is the place where the surgeon applies force. A casing for electronic

circuitry was attached to it, which was communicating with the wristband.

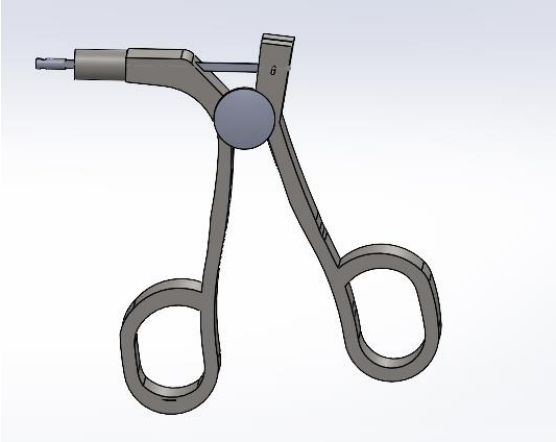

Figure 65. Handle of laparoscopic tool

### 4.11.2. Casing for Electronic circuitry

A casing was specially designed for the printing circuit board and the battery needed to power the circuit. It was specially designed for placing circuit boards.

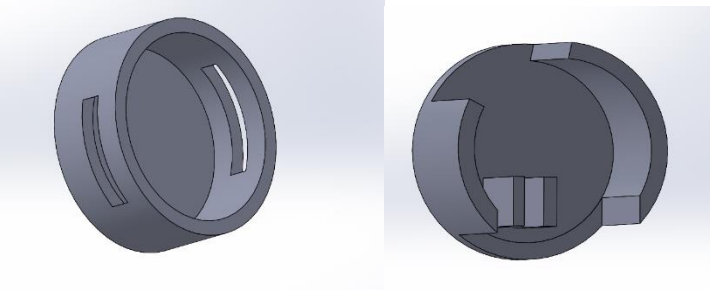

Figure 66. Casing for electronic circuit

### 4.11.3. Internal rod

A brass rod was used inside the tool to transfer the force of the handle to the gripping jaws for its motion. This was a straight rod attached at both ends to connect the handle with the mechanism of the grasper.

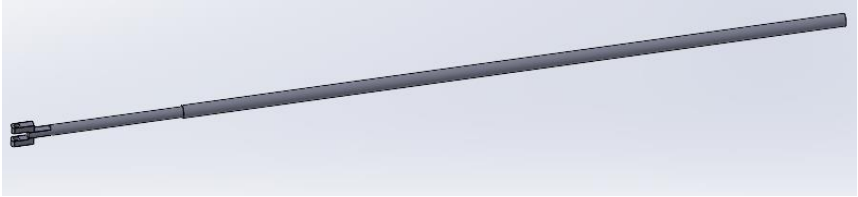

Figure 67. Internal brass rod

### 4.11.4. Grasper jaws (upper and lower)

The Grasper of the tool has two jaws i.e., upper, and lower. The lower jaw is static while the upper jaw is movable. It works on the mechanism of a single action.

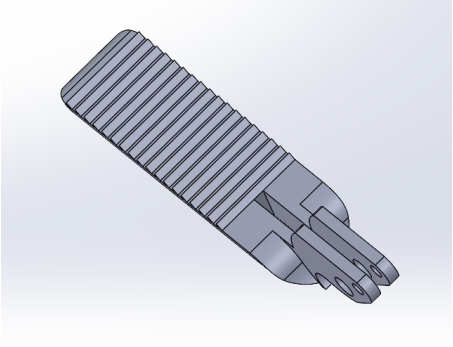

Figure 68. Upper jaw of the laparoscopic tool

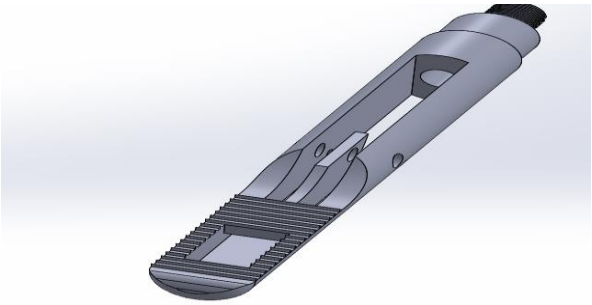

Figure 69: Lower Jaw of the Laparoscopic tool

# CHAPTER 5- SOFTWARE

This topic discusses the work done prior to real life implementation of the project, which is one of the most crucial steps of this project. Achieving the desired results on software enabled us to obtain our goals effortlessly in real life. Through Software implementation we have developed the project in SolidWorks to better visualize. This process includes the creation and assembly of our Smart Handheld Device. Then we use ANSYS to analyze and test out our designs before printing them. In addition to this, we test our sensor and actuator designs on appropriate tools, for better analysis of their working and limits.

## 5.1.Data Acquisition System

The Data Acquisition System for smart surgical tool is designed to incorporate two types of force data i.e., capacitive and resistive, the data acquisition for capacitive sensor is done using a 24-bit CDC (AD7746) is used (working has been described in the hardware section) and the data acquisition of resistive sensor is done using a 16-bit ADC. The data acquisition for the angle sensor is already designed by the manufacturer and its reliability and accuracy has been test, therefore the angular data from the position encoder (AS5600) is used with the resolution that was provided by the manufacturer i.e., $0.0879^{o}$.

### 5.1.1. Block Diagram of Data acquisition System

The system consists of the following standalone components:

i. Power Supply (5V battery)
ii. 3.3V level Shifter
iii. Microcontroller (ESP32-WROOM-32)
iv. AS5600 Position encoder
v. ADS1115 ADC
vi. AD7746 CDC
vii. Supporting circuitry

The block diagram of the system is shown below:

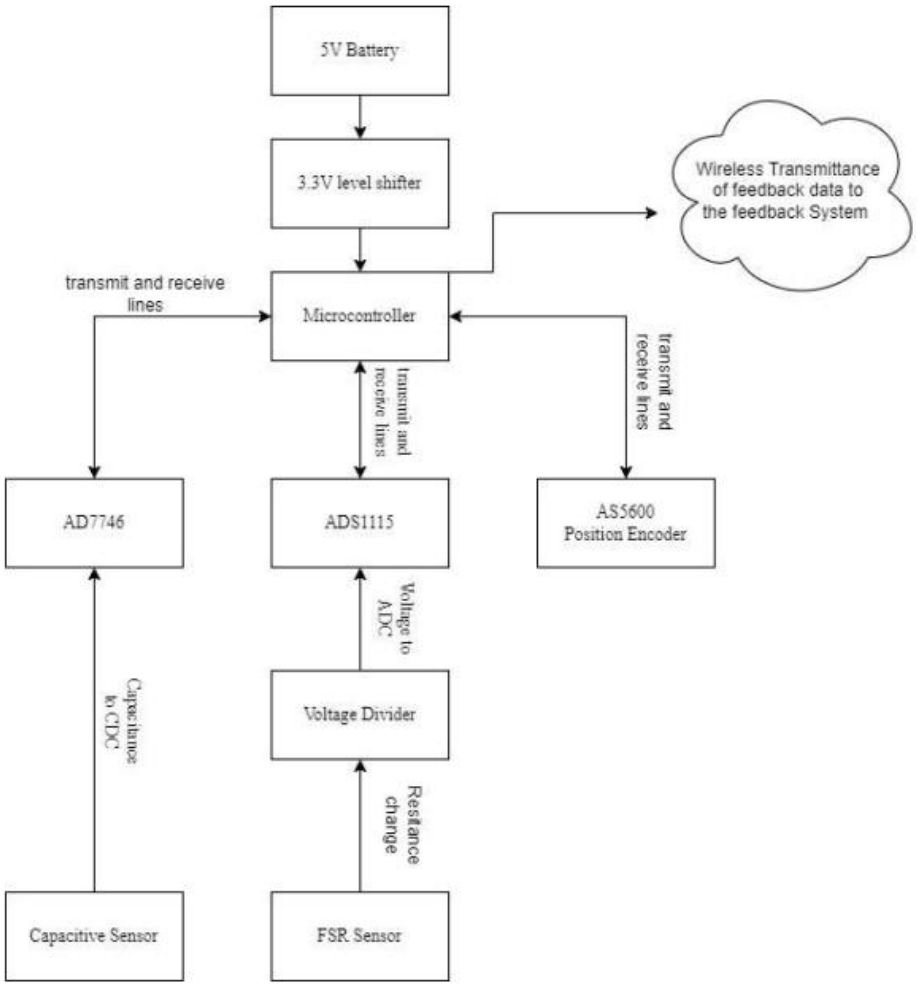


Figure 70. Block diagram of DAQ system

### 5.1.2. Circuit Schematics

The circuit design is mainly inspired by the datasheets of the standalone circuitry of ICs, there are several portions of the circuit that are performing a certain task. The whole schematics has been designed in EasyEDA software for its easy interface and powerful tools such as bill of materials facility (BOM), Gerber viewer, pick and place file for PCB assembly.

#### 5.1.2.1 Power Management

Overall data acquisition system is powered by a single 5V battery, and a level shifter is used to provide stable 3.3V to the whole circuit. The power management schematic is shown. The decoupling capacitors are

used to smoothen the power supply and to avoid any sudden voltage drops.

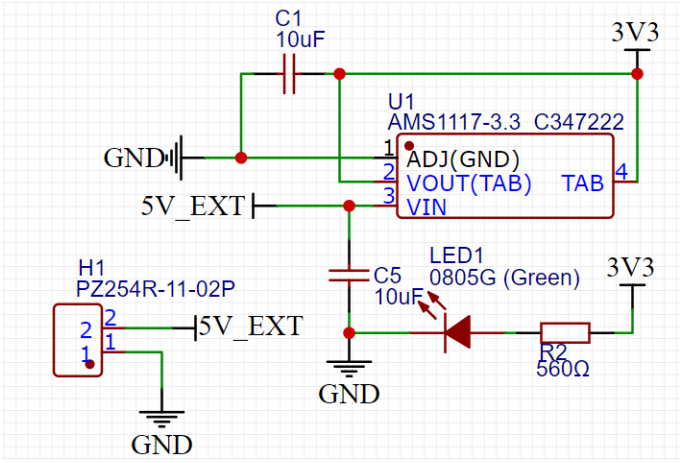


Figure 71. Power management circuitry

### 5.1.2.2 Microcontroller Circuit

This circuitry ensures the mode selection of ESP32 so that the microcontroller goes properly into boot mode and programming mode.

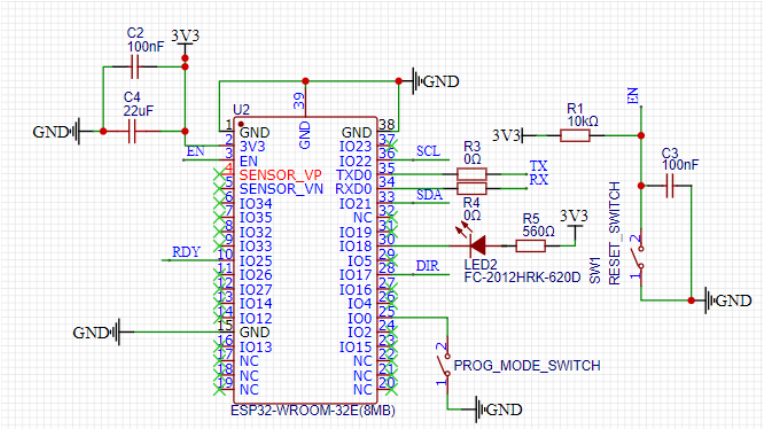


Figure 72. ESP32 supporting circuitry

### 5.1.2.3 Position Encoder Circuitry

This circuit is responsible for ensuring the attenuation of sudden voltage drops and provides proper communication between the encoder and the microcontroller.

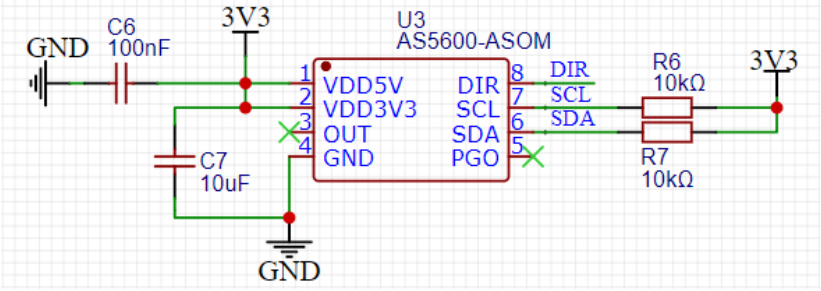


Figure 73. Position encoder supporting circuitry

#### 5.1.2.4 ADS1115 ADC Circuitry

This circuitry ensures the proper functionality by keeping the supply voltage stable as well as the communication bus circuitry for resistive force data acquisition.

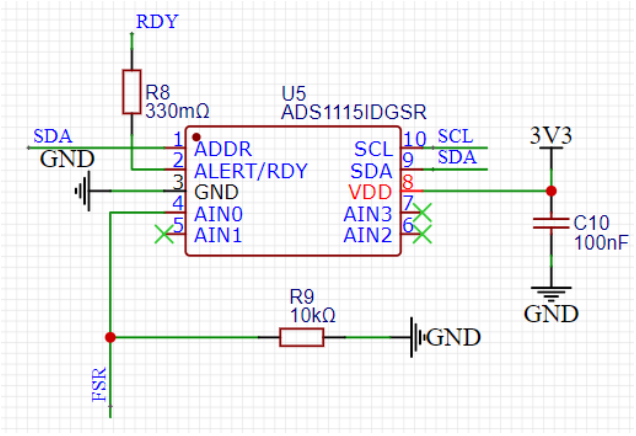


Figure 74. ADS1115 supporting circuitry

#### 5.1.2.5 AD7746 CDC Circuitry

This circuitry ensures the proper functionality by keeping the supply voltage stable as well as the communication bus circuitry for capacitive force data acquisition.

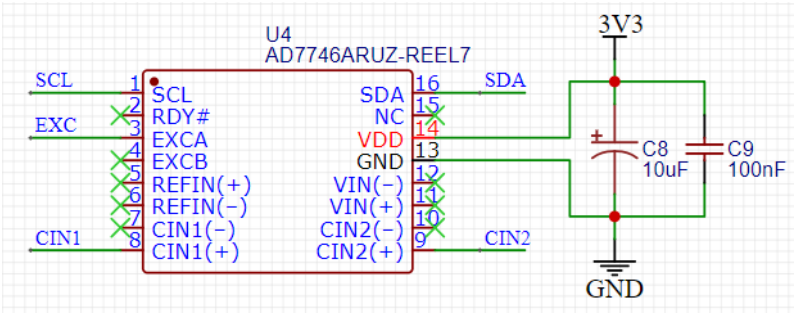


Figure 75. AD7746 supporting circuitry

### 5.1.3. PCB Design

The PCB is designed in four layers namely, Upper Layer, Inner1 Layer, Inner2 Layer, and Bottom Layer. The novel thing about the PCB is that it

decreases the size of our whole DAQ system by a factor of 3 as the standalone modules of above-mentioned ICs are a lot bigger in size relative to our PCB design. The PCB board has a radius of 42mm. The design of the PCB is shown.

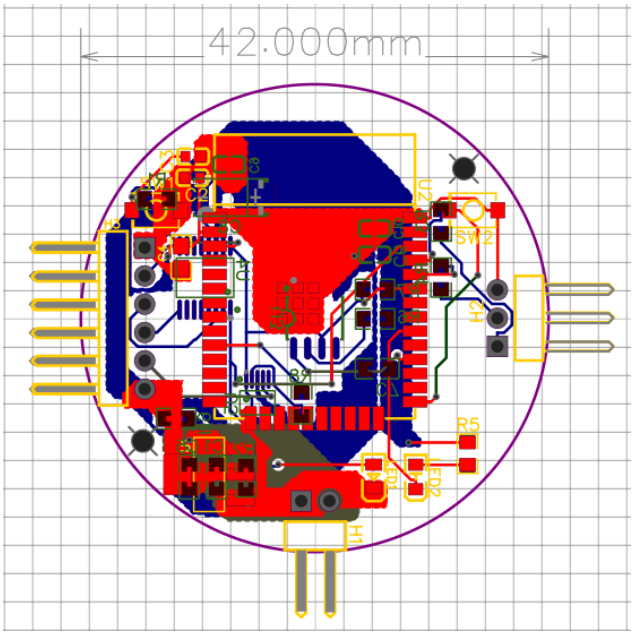


Figure 76. PCB design

### 5.1.4. 3D Model of PCB Design

3D model of the PCB is shown below. This is the actual form of how our data acquisition will turn out to be. The acquisition system is designed specifically to be mounted on the surgical tool design.

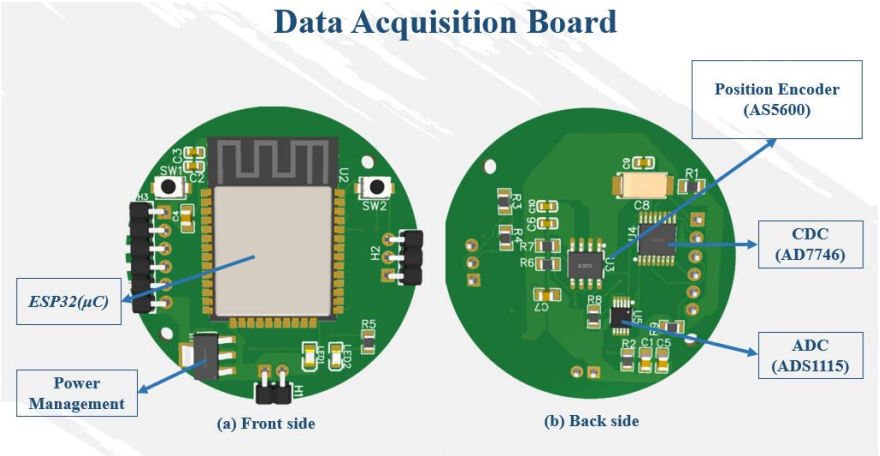


Figure 77. 3D Model of DAQ board

## 5.2.Modeling

Our project started off with the creation of 3D models of our device and its constituent parts. This helped us get a better idea of the sizes and materials as well as further performed analysis on them to get a better idea of their working before printing them. We designed our models on SolidWorks, a 3D Cad software. The objectives of this modeling consisted of:

i. Molds for sensor fabrication
ii. Hinge mechanism for force transmission
iii. Handheld device with Arduino, actuator placement, and hinge built into it

### 5.2.1. Molds for Sensor Fabrication

To fabricate our sensor, we followed a step-by-step process that involved curing polymers and assembling the dielectric between the electrodes. One crucial aspect was designing the appropriate molds for curing the polymers. We opted to use PLA material for 3D printing the molds, ensuring they were of the correct size and shape. Once the molds were ready, we carefully poured the desired polymer, Ecoflex 00-30, into one of the molds. This soft polymer served as the main component of the dielectric. We allowed the polymer to cure, ensuring it solidified and obtained the desired properties. Simultaneously, we prepared the upper and lower electrodes that would be placed above and below the dielectric. These electrodes would facilitate the measurement of capacitance changes. Moving forward, we proceeded to cure our second polymer, RTV-528 silicon rubber, in a separate mold. This hard polymer was used to create a pyramid-shaped dome that would be placed on top of the upper electrode.

Finally, we carefully joined the cured soft polymer with the hardened pyramid dome, creating the final structure of our sensor. The designs and structures of the molds, as well as the assembled sensor components, can be observed in the accompanying figures below.

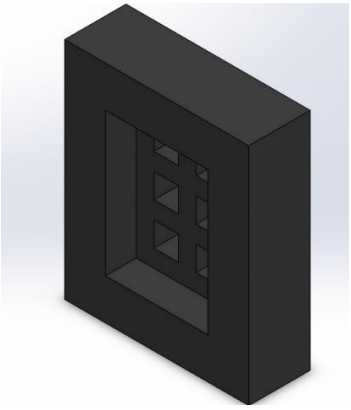

Figure 78. Mold for soft polymer

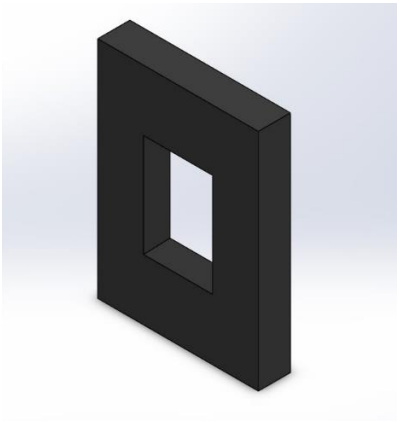

Figure 79. Mold for hard polymer

### 5.2.2. Sensor Modelling

Designing the sensor using SolidWorks allowed us to create a detailed and accurate representation of all its components. We incorporated the specifications required for the sensor to ensure that the design aligned with our intended functionality. By utilizing SolidWorks, we were able to perform various analyses and simulations on the virtual model of the sensor. This enabled us to evaluate its performance, identify potential areas for improvement, and make necessary adjustments before moving forward with the fabrication process. Through the analysis of the virtual model, we were able to assess factors like stress distribution, displacement, and capacitance changes under different applied forces. This analysis helped us refine the design and make informed decisions to enhance the sensor's efficiency and accuracy. Overall, the use of SolidWorks in the sensor design phase provided us with valuable insights and enabled us to optimize the design before proceeding with the physical fabrication.

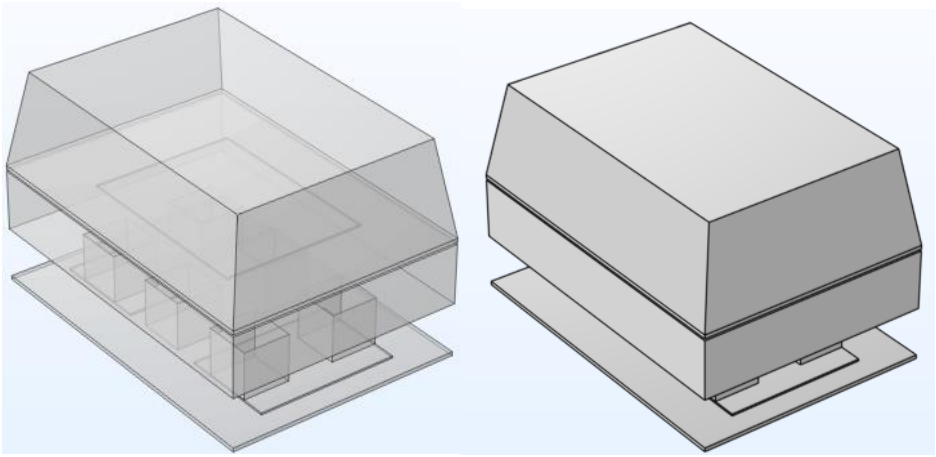

Figure 80. Sensor 3D model

### 5.3.Calibration

The calibration of FSR is very important, it means applying known force and checking the corresponding output of the sensor. It is very difficult task to calibrate FSR, due to the nature of FSR construction, its time dependency makes it hard to calibrate. We calibrated FSR sensor on Arduino IDE. Values were read from the sensor. The code for this calibration of the sensor is given in Appendix A.

### 5.4.Wireless Communication

The ESP32 microcontroller-based software implementation of the wireless force feedback communication system between a surgical tool and a smart haptic band is shown. The processes for gathering the force data from the surgical tool and wirelessly sending it to the receiver are described in the transmitter code (Appendix B). The process of collecting the force data and transforming it into haptic feedback signals is next illustrated by looking at the receiver code (Appendix C). Wi-Fi, the employed communication protocol, as well as the pertinent libraries and APIs needed for establishing and maintaining the wireless connection are discussed. Additionally, the implementation difficulties, enhancements, and any necessary alterations are highlighted in order to guarantee accurate and immediate force feedback.

### 5.5.Finite Element Analysis

It is very important to perform such analysis on the jaws of the laparoscopic tool to ensure the strength and damage that will occur on the moving jaw with the passage of time when it is used multiple times. For this very reason, we decided to carry out several mechanical analyses on the CAD model of our project. We designed the CAD models in SOLIDWORKS and then performed the respective analysis on ANSYS. Our main aim of the analysis was to determine the stress that appears on individual elements and deformation which would occur soon.

There are various types of analysis that can be performed on tools such as dynamic analysis and static analysis. The type of analysis we performed was Static structural analysis, in which we found stress, strain, and deformation in our grasper jaw under load conditions. Structural loads are a combination of:

i. External Forces
ii. Surface Loads
iii. Body Forces

Our analysis started with importing the static structural feature into ANSYS. After that, we moved to the engineering data section, where we set our material properties. Our grasper Material was engineering resin. We added a new material named engineering resin and then we added their properties as follows.

Properties of Outline Row 4: Resin Polyester

| | A | B | C | D | E |
|---|---|---|---|---|---|
| 1 | Property | Value | Unit | | |
| 2 | Material Field Variables | Table | | | |
| 3 | Density | 110 | g cm^-3 | | |
| 4 | Isotropic Elasticity | | | | |
| 5 | Derive from | Young's Modu... | | | |
| 6 | Young's Modulus | 1.8 | GPa | | |
| 7 | Poisson's Ratio | 0.35 | | | |
| 8 | Bulk Modulus | 2E+09 | Pa | | |
| 9 | Shear Modulus | 6.6667E+08 | Pa | | |
| 10 | Tensile Yield Strength | 4.85E-05 | MPa | | |
| 11 | Viscosity | 0.000365 | MPa s | | |

Figure 81. Engineering data for grasper analysis

Afterwards, we continue with our analysis. We assigned the properties of the material we made earlier to the geometry and then moved toward the meshing part. Meshing is basically a process in which a complex geometry is divided into smaller parts, each part called a mesh element to perform better analysis on each individual part. For better meshing, we tried to keep the mesh size smaller which was 2. Our geometry after meshing appeared as:

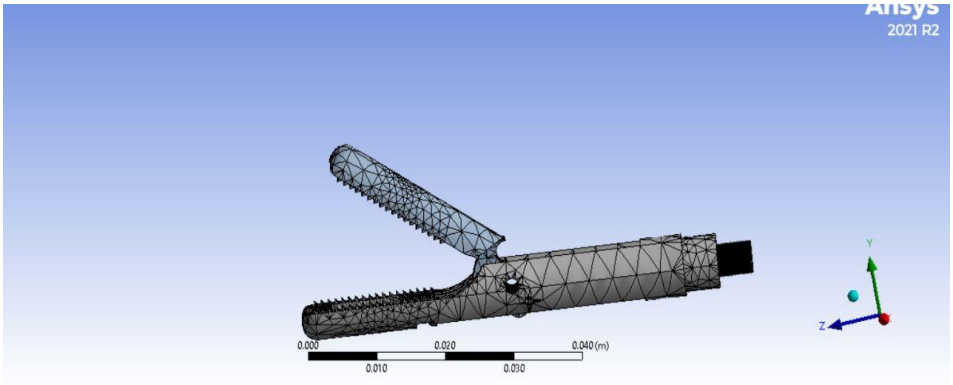


Figure 82: Meshing of the grasper

Now we moved towards the part where we need to apply different required forces, loads, and set fixed support. It is necessary for every structure to have fixed support. The body which is set as fixed support is immovable and the remaining parts move across that body. So, we set the lower jaw as fixed support because it is fixed in single action grasper and the upper jaw which is attached to it moves.

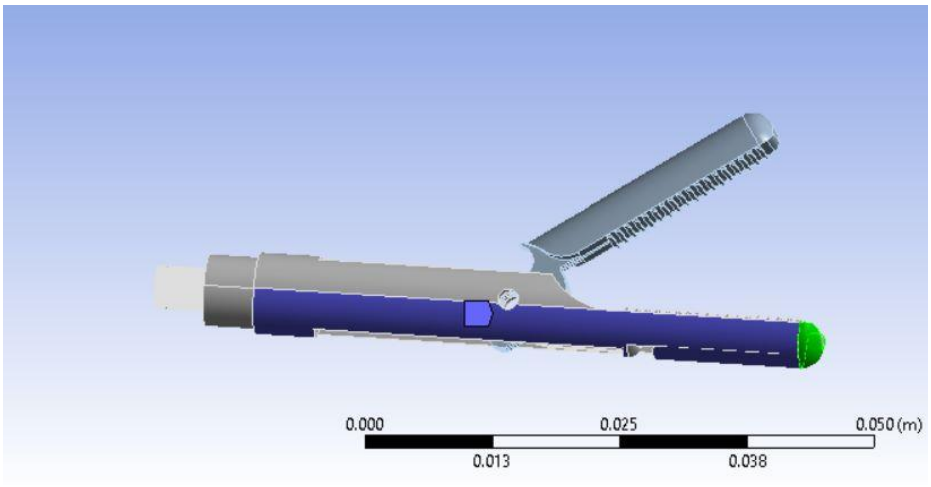


Figure 83: Fixed support for grasper

After setting the lower jaw as fixed support, we apply forces that rotate the upper jaw. Two forces are applied to the extended part of the upper jaw which is basically pulling the jaw for closing the grasper and pushing the jaw for opening the grasper.

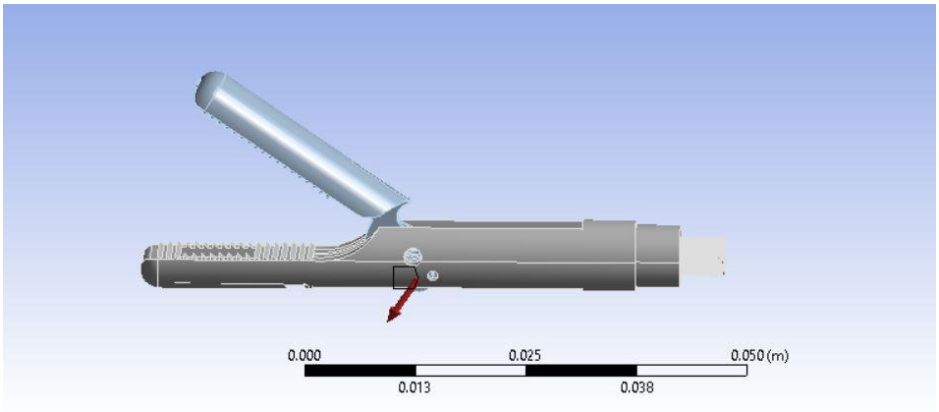


Figure 84: Forces applied on upper jaw for motion

After the application of forces, we inserted the required solution which was total deformation and equivalent stress. The results of analysis are shown in the following chapter.

# CHAPTER 6- RESULTS

This chapter describes the results achieved as part of the dissertation. This section describes the LabVIEW model for sensor testing, Hinge design and analysis on Ansys, and Arduino testing for EDM motors developed during this phase.

## 6.1.Capacitive Sensor Testing

Testing the sensor using the AD7746 CDC Board was an essential step in evaluating its performance and functionality. The board allowed us to interface with the sensor and collect data for analysis. During this testing process, we focused on assessing the sensor's response to both normal and shear forces. To conduct the tests, we wrote specific code to interface with the AD7746 CDC Board and retrieve the sensor data. The code was designed to capture the output from the sensor and display it graphically, enabling us to visualize the results. During the testing phase, we applied normal forces to the sensor by using a push-pull force mechanism. This validation step assured us that the sensor was functioning correctly and could receive input and provide output accordingly. Overall, the testing process using the AD7746 CDC Board provided us with valuable data to assess the sensor's performance and verify its accuracy in measuring both normal and shear forces.

### 6.1.1. Output

A jig was used to hold the sensor. The CNC machine was equipped with a push-pull gauge that delivered force to the sensor's tip. The graph shows that the sensor performed as intended. The force applied in Normal direction is from 0 to 10 N and 3 N in Shear direction.

Table 18. Results of Shear Force

| F | C1 | C2 |
|---|---|---|
| 0 | 0.01835 | 0.0208 |
| 0.5 | 0.01704 | 0.02243 |
| 1 | 0.01609 | 0.02348 |
| 1.5 | 0.01519 | 0.02481 |
| 2 | 0.01381 | 0.02551 |
| 2.5 | 0.01275 | 0.02779 |
| 3 | 0.01221 | 0.03055 |

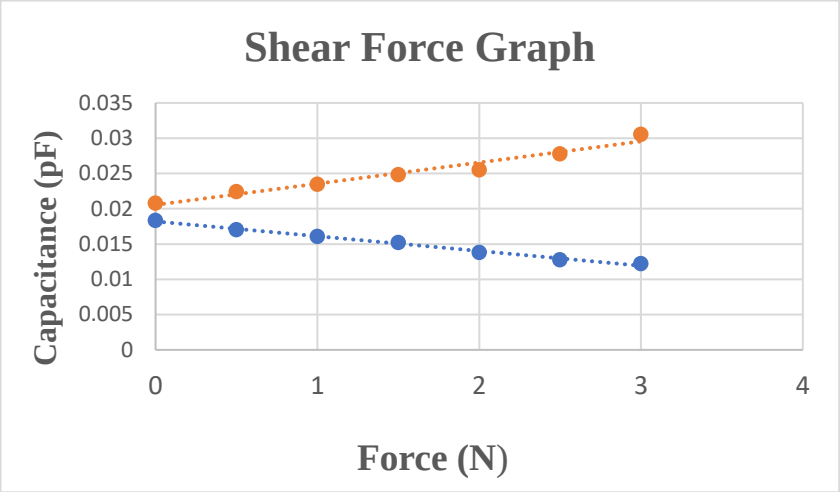


Figure 85. Shear force vs capacitance graph

Table 19. Results of Normal Force

| Force | Average Capacitance |
|---|---|
| 0 | 0.04216 |
| 0.5 | 0.043035 |
| 1 | 0.04506 |
| 1.5 | 0.047605 |
| 2 | 0.048835 |
| 2.5 | 0.050005 |
| 3 | 0.053485 |
| 3.5 | 0.05488 |
| 4 | 0.05531 |
| 4.5 | 0.05621 |
| 5 | 0.05765 |
| 5.5 | 0.058475 |
| 6 | 0.05901 |
| 6.5 | 0.06054 |
| 7 | 0.061745 |
| 7.5 | 0.063195 |
| 8 | 0.06441 |
| 8.5 | 0.06549 |
| 9 | 0.066285 |
| 9.5 | 0.066405 |
| 10 | 0.067625 |

However, since the elastomer was getting deformed keeping in detail of accuracy only till 10 N has been considered in results. The results in Normal direction are:

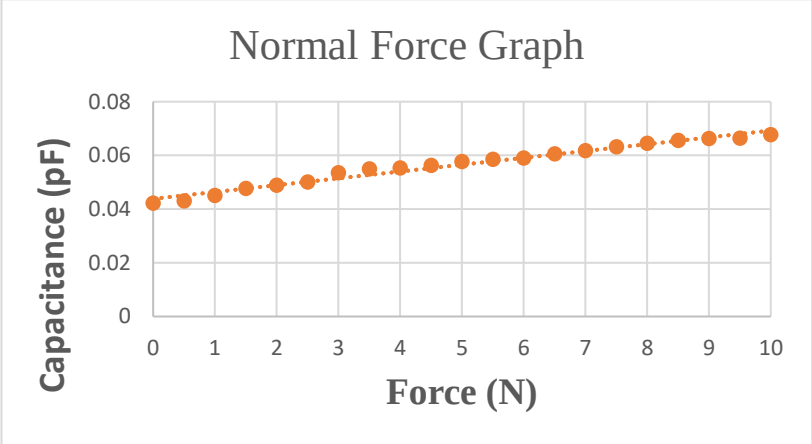


Figure 86. Normal force vs capacitance graph

## 6.2.Electromechanics Analysis

COMSOL was used to simulate the electromechanics behavior of the sensor. It gives the force relationship with capacitance and force relationship with displacement.

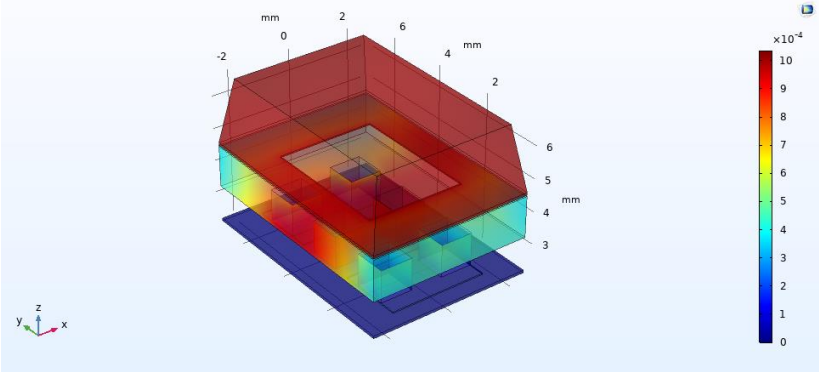


Figure 87. Simulation modeling and deformation results under normal force with applied force range of (0-10 N)

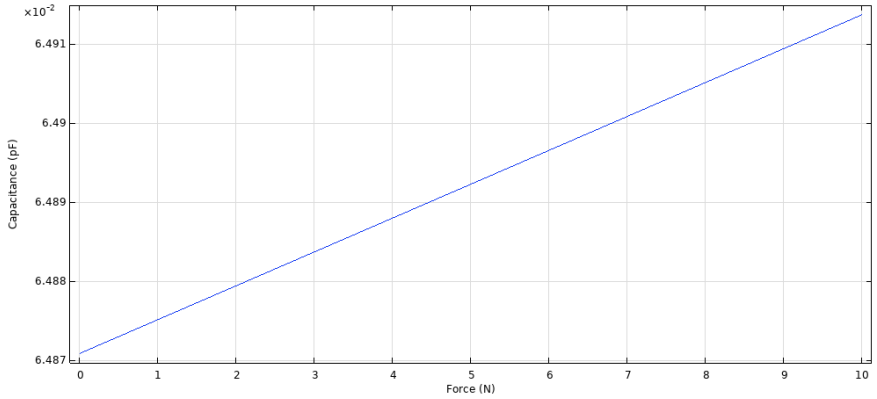


Figure 88. Relationship graph between capacitance and normal force

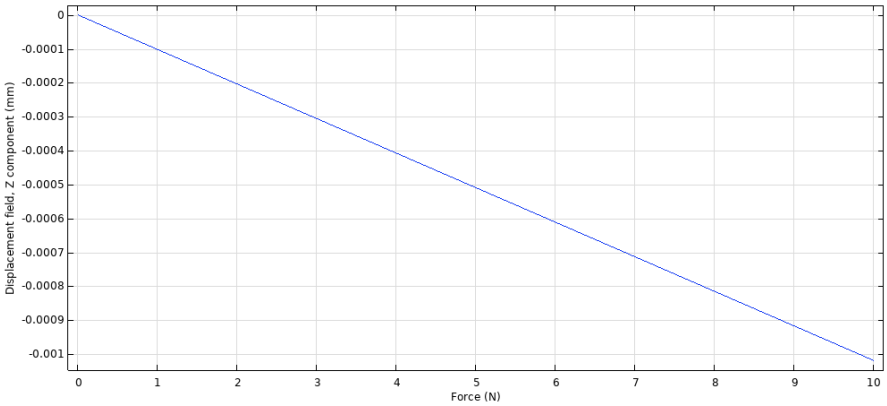


Figure 89. Relationship graph between displacement and normal force

### 6.3.FSR Calibration

The CNC machine was equipped with a push-pull gauge that delivered force to the sensor's tip. The stage's motor was controlled. When the force is applied, the change in resistance causes corresponding voltage to change in voltage divider circuit. This change is detected by 16-bit external ADC (ADS1115), and the final digital output is shown on the serial monitor. Force is applied from 0-20N. The average value is taken because of the changing value of the FSR on the same applied force.

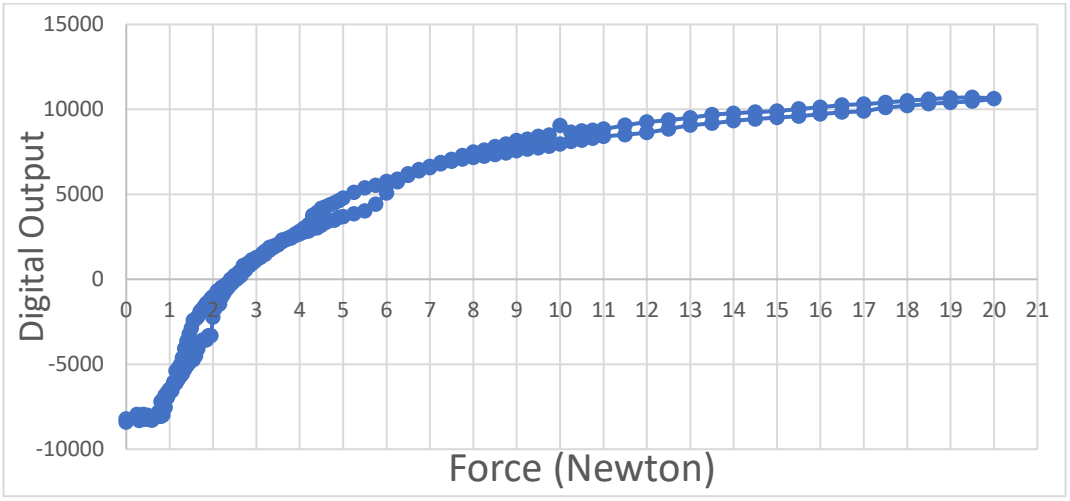


Figure 90. Force vs. Digital Output

## 6.4.Ansys Analysis of Laparoscopic tool grasper

Grasper is the most important part of laparoscopic tool because it has direct contact with tissue of the patient's body. So, analysis was performed on this part of the tool. The grasper was designed using Solidworks and then ANSYS software was used for its analysis. The result of analysis was quite good as shown below:

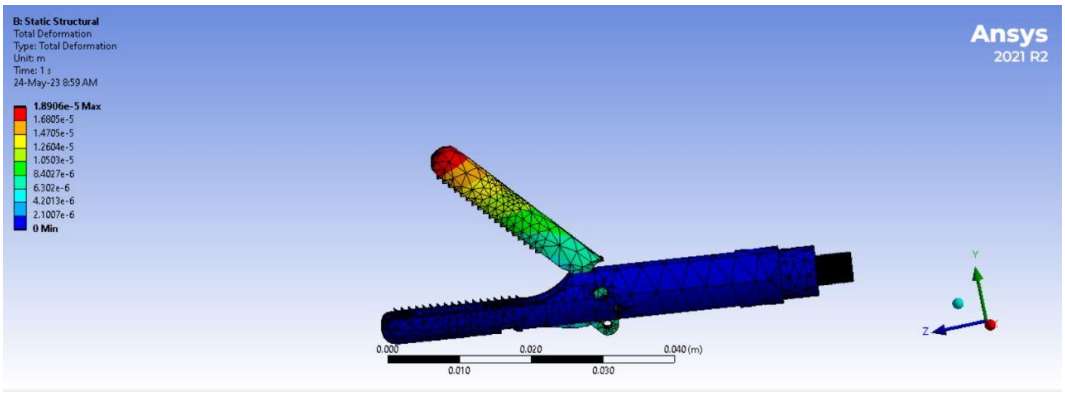


Figure 91. Total deformation results

# CHAPTER 7- CONCLUSION AND FUTURE WORK

## 7.1. Design Modification

The design of the present tool is good enough to carry out the necessary operation and fulfill surgeons' needs but in future we will modify our design to make it more compact and will make it safer to perform operations. Sensor slot will be made compact and fully enclosed. Also, the electrical wiring would be perfectly covered so that there is zero chance of any type of damage to the patient's body. Our existing tool size is a little bit big so we will make it smaller for minimal invasion and fast recovery. The handle of tool would be made more comfortable to reduce surgeon's fatigue.

## 7.2. Circuit Modification

In the field of design, one thing that everyone agrees on is that there can always be a better design than the existing one. Therefore, here are areas in which future research can make a lot of difference in the current design of data acquisition system. Our future approach will be to research on better and more sensitive electronic ICs to acquire maximum undistorted data to generate a stable and correct response on the feedback end. One of the most crucial research areas is the power management of the acquisition system so that the power supply lasts longer during actual surgical operations.

## 7.3. Sensor modification

The differential capacitances varied due to fabrication factors like thickness variations in the dielectric layer, curing and peel-off process inconsistencies, and physical dimension variations of the posts caused by trapped air bubbles. These variations affected the initial capacitance and the local dielectric index of the unit cells. Alignment errors between the top and bottom electrodes also contributed to overlap area variations. Custom alignment marks and holding jigs with posts improved alignment, while high-resolution molds and hydrophobic coatings enhanced uniformity in the dielectric layer by facilitating the release and movement of trapped air bubbles.

To estimate the out-of-plane force angle, the spring constant of the patterned dielectric layer needed to be determined. This involved mechanically characterizing the dielectric layer and tracking the displacement of the top electrode layer in all three axes relative to the bottom electrode layer.

## 7.4.Integration With Surgical Robotic System

To enhance the smart surgical tool, prioritize seamless integration with existing surgical tools and systems. This entails developing standardized interfaces and protocols for smooth connection and communication between the smart tool and established equipment. Collaborate with surgical system manufacturers to ensure compatibility and establish integration guidelines.

Design the smart surgical tool to be adaptable and flexible, capable of interfacing with various surgical instruments and robotic platforms. Thorough research and

engineering are necessary to address challenges such as differing communication protocols, mechanical interfaces, and control mechanisms. Consider usability and ergonomic factors to ensure user-friendly integration that doesn't disrupt the surgical workflow. Strive for seamless integration that requires minimal modifications or adjustments to the existing setup.

Regularly test and validate the integrated system to ensure performance, reliability, and safety. Conduct comprehensive preclinical studies and engage surgeons and healthcare professionals for valuable feedback and evaluation.

Successful integration of the smart surgical tool with existing tools enables benefits such as enhanced capabilities, improved accuracy, and expanded functionalities. Surgeons can leverage the advanced features and technologies of the smart tool within their existing surgical setups, leading to enhanced patient outcomes and advancements in minimally invasive surgery.

## 7.5.Conclusion

The implementation of artificial tactile sensation in laparoscopic tools can address the challenges associated with indirect tissue handling. By restoring the sense of touch, surgeons can gain valuable information about applied forces and tissue stiffness, which in turn enables various benefits such as lump detection, pressure estimation on thin tissue walls, and informed decision-making during surgical procedures. This study serves as a proof-of-concept, showcasing the effectiveness of the proposed concept using smart laparoscopic grasping forceps equipped with off-the-shelf sensors. Real-time feedback on two important grasping parameters, namely the grasping force and angle of deformation, is provided through these sensors. The demonstrated capability to estimate the stiffness of grasped samples or objects based on this feedback is a significant advancement.

Moreover, the in-house developed prototype of the smart laparoscopic tool proved to be an asset for surgeons. It assisted in determining the appropriate amount of force applied to grasped tissues, leading to improved hand-device coordination and more accurate sample sorting based on hardness. Additionally, this approach holds promise for tumor detection developments, as it can provide insights into hidden lumps by indicating the location of stiffer, unhealthy segments. When combined with novel imaging devices, this approach can further enhance the visualization and identification of tumors and other abnormalities.

Overall, this work demonstrates the potential of integrating artificial tactile sensation into laparoscopic tools to enhance surgical procedures and provide surgeons with vital feedback and information. Continued advancements in this field can lead to improved surgical outcomes, increased surgeon confidence, and further developments in tumor detection and characterization.

# APPENDIX A

```
#include <Adafruit_ADS1X15.h>
#include <math.h>

double y;
double x;

Adafruit_ADS1115 ads;
constexpr int READY_PIN = 3;


#ifndef IRAM_ATTR
#define IRAM_ATTR
#endif

int a,b,c,d,e,f,g,h,i,j = 0;
long int average1 =0;
long int average2 =0;
long int average3 =0;
long int AVERAGE =0;
volatile bool new_data = false;
void IRAM_ATTR NewDataReadyISR() {
new_data = true;
}

void setup(void)
{
Serial.begin(115200);
ads.setGain(GAIN_ONE);        // 1x gain   +/- 4.096V  1 bit = 2mV      0.125mV
if (!ads.begin()) {
Serial.println("Failed to initialize ADS.");
while (1);
}
pinMode(READY_PIN, INPUT);
attachInterrupt(digitalPinToInterrupt(READY_PIN), NewDataReadyISR, FALLING);
ads.startADCReading(ADS1X15_REG_CONFIG_MUX_DIFF_0_1,
/*continuous=*/true);
}

void loop(void)
{
```

```
int16_t results = ads.getLastConversionResults();
new_data = false;
a=results;
delay(30);
b=results;
delay(30);
c=results;
delay(30);
d=results;
delay(30);
e=results;
delay(30);
f=results;
delay(30);
g=results;
delay(30);
h=results;
delay(30);
i=results;
delay(30);
j=results;
delay(30);
average1 = (a+b+c);
average2 = (d+e+f);
average3 = (g+h+i);
AVERAGE= average1+average2+average3+j;
AVERAGE = AVERAGE/10;

y = AVERAGE;
if (y<-8300)
{
x=0;
}
else if (y>-8300 && y<-8080)
{
x = (sqrt((y + 8100.95)/-716.79)) + 0.52191;
}
else if (y>-8080 && y<-3700)
{
x = (0.02773*sqrt(y + 11796.8018)) - 0.9875;
}
else if (y>-3700 && y< 4000)
```

```
{
x= -(sqrt((y - 4033.0417)/(-499.83))) + 5.40943;
}
else if ( y> 4000)
{
x= -(sqrt((y - 10313.44017)/(-32.3))) + 18.10990;
}
else
{
x= (sqrt((y - 11042.20791)/(-97.417))) + 13.86257;
//x=0;
}

Serial.println(y);
delay(100);
}
```

# APPENDIX B

```
#include <esp_now.h>
#include <WiFi.h>
#include <Wire.h>
#include <Adafruit_ADS1X15.h>
#include <math.h>

double y;
double x;

Adafruit_ADS1115 ads;
constexpr int READY_PIN = 10;

#ifndef IRAM_ATTR
#define IRAM_ATTR
#endif

int a, b, c, d, e, f, g, h, i, j = 0;
long int average1 = 0;
long int average2 = 0;
long int average3 = 0;
long int AVERAGE = 0;

volatile bool new_data = false;

void IRAM_ATTR NewDataReadyISR() {
  new_data = true;
}

uint8_t RxMACaddress[] = {0x7C, 0x9E, 0xBD, 0x66, 0x27, 0xA8};

typedef struct TxStruct {
  int potVal;
} TxStruct;

TxStruct sentData;

void OnDataSent(const uint8_t *mac_addr, esp_now_send_status_t status) {
  Serial.print("\r\nLast Packet Send Status:\t");
  Serial.println(status == ESP_NOW_SEND_SUCCESS ? "Delivery Success" :
"Delivery Fail");
```

```
}

void setup() {
  Serial.begin(9600);
  WiFi.mode(WIFI_STA);

  if (esp_now_init() != ESP_OK) {
    Serial.println("Error initializing ESP-NOW");
    return;
  }

  esp_now_register_send_cb(OnDataSent);

  esp_now_peer_info_t peerInfo;
  memcpy(peerInfo.peer_addr, RxMACaddress, 6);
  peerInfo.channel = 0;
  peerInfo.encrypt = false;

  if (esp_now_add_peer(&peerInfo) != ESP_OK) {
    Serial.println("Failed to add peer");
    return;
  }

  ads.setGain(GAIN_ONE);

  if (!ads.begin()) {
    Serial.println("Failed to initialize ADS.");
    while (1);
  }

  pinMode(READY_PIN, INPUT);
  attachInterrupt(digitalPinToInterrupt(READY_PIN), NewDataReadyISR,
FALLING);
  ads.startADCReading(ADS1X15_REG_CONFIG_MUX_DIFF_0_1,
/*continuous=*/true);
}

void loop() {
  int16_t results = ads.getLastConversionResults();
  new_data = false;
  a = results;
  delay(30);
```

```
  results = ads.getLastConversionResults();
  b = results;
  delay(30);
  results = ads.getLastConversionResults();
  c = results;
  delay(30);
  results = ads.getLastConversionResults();
  d = results;
  delay(30);
  results = ads.getLastConversionResults();
  e = results;
  delay(30);

  results = ads.getLastConversionResults();
  f = results;
  delay(30);
  results = ads.getLastConversionResults();
  g = results;
  delay(30);
  results = ads.getLastConversionResults();
  h = results;
  delay(30);
  results = ads.getLastConversionResults();
  i = results;
  delay(30);
  results = ads.getLastConversionResults();
  j = results;
  delay(30);
  average1 = (a + b + c);
  average2 = (d + e + f);
  average3 = (g + h + i);
  AVERAGE = average1 + average2 + average3 + j;
  AVERAGE = AVERAGE / 10;
  y = AVERAGE;
  sentData.potVal = y;
  esp_err_t result = esp_now_send(RxMACaddress, (uint8_t *)&sentData,
sizeof(sentData));
  if (result == ESP_OK) {
    Serial.println("Sent with success");
  } else {
    Serial.println("Error sending the data");
  }}
```

# APPENDIX C

```
#include <esp_now.h>
#include <WiFi.h>

const int pwmPin = 19;
const int pwmPin2 = 18;
double y;

typedef struct RxStruct {
  int potVal;
} RxStruct;

RxStruct receivedData;

void OnDataRecv(const uint8_t *mac, const uint8_t *incomingData, int len) {
  memcpy(&receivedData, incomingData, sizeof(receivedData));
}

void setup() {
  Serial.begin(9600);

  ledcAttachPin(pwmPin, 0);
  ledcSetup(0, 5000, 8);
  ledcAttachPin(pwmPin2, 1);
  ledcSetup(1, 5000, 8);

  WiFi.mode(WIFI_STA);

  if (esp_now_init() != ESP_OK) {
    Serial.println("Error initializing ESP-NOW");
    return;
  }

  esp_now_register_recv_cb(OnDataRecv);
}

void loop() {
  y = receivedData.potVal;

  if (y > 30000) {
    ledcWrite(0, 0);
```

```
    ledcWrite(1, 0);
  } else if (y < 30000 && y > 20000) {
    ledcWrite(0, 100);
    ledcWrite(1, 100);
  } else if (y < 20000 && y > 10000) {
    ledcWrite(0, 170);
    ledcWrite(1, 170);
  } else if (y < 10000) {
    ledcWrite(0, 255);
    ledcWrite(1, 255);
  }
}
```

# REFERENCES


[1] Okamura AM. “Haptic feedback in robot-assisted minimally invasive surgery.” Curr Opin Urol. 2009 Jan;19(1):102-7. doi: 10.1097/MOU.0b013e32831a478c. PMID: 19057225; PMCID: PMC2701448.

[2] van der Meijden, O.A.J., Schijven, M.P. “The value of haptic feedback in conventional and robot-assisted minimal invasive surgery and virtual reality training: a current review.” *Surg Endosc* 23, 1180–1190 (2009).

[3] C. R. Wagner, N. Stylopoulos, P. G. Jackson and R. D. Howe, "The Benefit of Force Feedback in Surgery: Examination of Blunt Dissection," in Presence, vol. 16, no. 3, pp. 252-262, 1 June 2007, doi: 10.1162/pres.16.3.252.

[4] Jumpiei Arata, Shogo Terakawa, Hideo Fujimoto, “Fiber Optic Force Sensor for Medical Applications within a Backbone-shape Structure”, Procedia CIRP, Volume 5, 2013, Pages 66-69, ISSN 2212-8271

[5] Morris B. “Robotic surgery: applications, limitations, and impact on surgical education.” MedGenMed. 2005 Sep 27;7(3):72. PMID: 16369298; PMCID: PMC1681689.

[6] Kuo, CH., Dai, J.S. (2009). “Robotics for Minimally Invasive Surgery: A Historical Review from the Perspective of Kinematics”. In: Yan, HS., Ceccarelli, M. (eds) International Symposium on History of Machines and Mechanisms. Springer, Dordrecht.

[7] Ray Garry, “Laparoscopic surgery, Best Practice & Research Clinical Obstetrics & Gynaecology”, Volume 20, Issue 1,2006, Pages 89-104, ISSN 1521-6934,

[8] Journal Article Mack, Michael J. “Minimally Invasive and Robotic Surgery” JAMA 2001 10.1001/jama.285.5.568

[9] Park AE, Mastrangelo MJ, Gandsas A, Chu U, Quick NE. “Laparoscopic Dissecting Instruments”. Seminars in Laparoscopic Surgery. 2001;8(1):42-52

[10] JOUR “A laparoscopic grasper with force perception Herder”, J. L. Horward, M. J. Sjoerdsma, W.1997/01/01

[11] Driessen, S.R.C., Sandberg, E.M., Rodrigues, S.P. *et al.* “Identification of risk factors in minimally invasive surgery: a prospective multicenter study”. *Surg Endosc* 31, 2467–2473 (2017)

[12] Sawada, A. *et al.* (2018). “Laparoscopic Forceps with Force Feedback”. In: Kurosu, M. (eds) Human-Computer Interaction. Interaction in Context. HCI 2018. Lecture Notes in Computer Science(), vol 10902. Springer, Cham

[13] Khandalavala, Karl, et al. "Emerging surgical robotic technology: a progression toward microbots." *Ann Laparosc Endosc Surg* 5.0 (2020): 3

[14] W. Othman et al., "Stiffness Assessment and Lump Detection in Minimally Invasive Surgery Using In-House Developed Smart Laparoscopic Forceps," in IEEE Journal of Translational Engineering in Health and Medicine, vol. 10, pp. 1-10, 2022, Art no. 2500410, doi: 10.1109/JTEHM.2022.3180937

[15] G. Tholey and J. P. Desai, "A Modular, Automated Laparoscopic Grasper with Three-Dimensional Force Measurement Capability," Proceedings 2007 IEEE International Conference on Robotics and Automation, 2007, pp. 250-255, doi:

10.1109/ROBOT.2007.363795

[16] Nguyen, T., Dinh, T., Phan, H.P., Pham, T.A., Nguyen, N.T. and Dao, D.V., 2021. "Advances in ultrasensitive piezoresistive sensors: from conventional to flexible and stretchable applications". *Materials Horizons*

[17] Kumar, S.S. and Pant, B.D., 2014. "Design principles and considerations for the 'ideal'silicon piezoresistive pressure sensor: a focused review". Microsystem technologies, 20(7), pp.1213-1247.

[18] Fiorillo, A.S., Critello, C.D. and Pullano, S.A., 2018. Theory, technology and applications of piezoresistive sensors: A review. *Sensors and Actuators A: Physical*, *281*, pp.156-175.

[19] Othman, W., Vandyck, K.E., Abril, C., Barajas-Gamboa, J.S., Pantoja, J.P., Kroh, M. and Qasaimeh, M.A., 2022. Stiffness Assessment and Lump Detection in Minimally Invasive Surgery Using In-House Developed Smart Laparoscopic Forceps. *IEEE Journal of Translational Engineering in Health and Medicine*.

[20] Kim, U., Lee, D.H., Yoon, W.J., Hannaford, B. and Choi, H.R., 2015. "Force sensor integrated surgical forceps for minimally invasive robotic surgery". *IEEE Transactions on Robotics*, *31*(5), pp.1214-1224.

[21] Sreenath, V. and George, B., 2018. "A robust switched-capacitor CDC". *IEEE Sensors Journal*, *18*(14), pp.5985-5992.

[22] Li, R., Chen, Y., Tan, Y., Zhou, Z., Li, T. and Mao, J., 2018. "Sensitivity enhancement of FBG-based strain sensor." *Sensors*, *18*(5), p.1607.

[23] Sun, K., Li, M., Wang, S., Zhang, G., Liu, H. and Shi, C., 2021. "Development of a fiber Bragg grating-enabled clamping force sensor integrated on a grasper for laparoscopic surgery". *IEEE Sensors Journal*, *21*(15), pp.16681-16690.

[24] Volkmar Falk, Thomas Walther, Friedrich W. Mohr, "Minimally Invasive Cardiac Surgery," Industrial Robot", Robotics and Telemanipulation, chp 31, pp. 445–459

[25] Claudio Melchiorri, "ROBOTIC TELEMANIPULATION SYSTEMS: AN OVERVIEW ON CONTROL ASPECTS", IFAC Proceedings Volumes, Volume 36, Issue 17, 2003, Pages 21-30, ISSN 1474-6670,

[26] AMAL ELAWAD,"Stability Analysis of Haptic Teleoperation Systems Undergoing Delays in Robot-Assisted Telesurgery", 2017

[27] Prof. Dr. Franziska Mathis-Ullrich,"Telemanipulation in Robotic Surgery", Control of a Redundant Robot under Motion Restrictions, pp. 1

[28] A.R. Lanfranco, A. E. Castellanos, J. P.Desai, andW.C.Meyers, "Robotic surgery," Annal. Surgery, vol. 239, pp. 14–21, 2004.

[29] Othman W, Lai ZA, Abril C, Barajas-Gamboa JS, Corcelles R, Kroh M, Qasaimeh MA.

“Tactile Sensing for Minimally Invasive Surgery: Conventional Methods and Potential Emerging Tactile Technologies”. Front Robot AI. 2022 Jan 7;8:705662. doi: 10.3389/frobt.2021.705662. PMID: 35071332; PMCID: PMC8777132.

[30] Reiley CE, Akinbiyi T, Burschka D, Chang DC, Okamura AM, Yuh DD. “Effects of visual force feedback on robot-assisted surgical task performance”. J Thorac Cardiovasc Surg. 2008 Jan;135(1):196-202. doi: 10.1016/j.jtcvs.2007.08.043. PMID: 18179942; PMCID: PMC2674617.

[31] Freschi C, Ferrari V, Melfi F, Ferrari M, Mosca F, Cuschieri A. “Technical review of the da Vinci surgical telemanipulator.” Int J Med Robot. 2013 Dec;9(4):396-406. doi: 10.1002/rcs.1468. Epub 2012 Nov 20. PMID: 23166047.

[32] Okamura AM. "Haptic feedback in robot-assisted minimally invasive surgery". Curr Opin Urol. 2009 Jan;19(1):102-7. doi: 10.1097/MOU.0b013e32831a478c. PMID: 19057225; PMCID: PMC2701448.

[33] Henri Boessenkool, David A. Abbink, Cock J.M. Heemskerk, Frans C.T. van der Helm, and Jeroen G.W. Wildenbeest,"A Task-Specific Analysis of the Benefit of Haptic Shared Control During Telemanipulation", pp. 2, 2012

[34] Ouyang Q, Wu J, Sun S, Pensa J, Abiri A, Dutson E, Bisley J. “Bio-Inspired Haptic Feedback for Artificial Palpation in Robotic Surgery”. IEEE Trans Biomed Eng. 2021 Oct;68(10):3184-3193. doi: 10.1109/TBME.2021.3076094. Epub 2021 Sep 20. PMID: 33905321; PMCID: PMC8486347

[35] V. Pruks and J. -H. Ryu, "A Framework for Interactive Virtual Fixture Generation for Shared Teleoperation in Unstructured Environments," 2020 IEEE International Conference on Robotics and Automation (ICRA), 2020, pp. 10234-10241, doi: 10.1109/ICRA40945.2020.9196579.

[36] J. J. Abbott and A. M. Okamura, "Virtual fixture architectures for telemanipulation," 2003 IEEE International Conference on Robotics and Automation (Cat. No.03CH37422), 2003, pp. 2798-2805 vol.2, doi: 10.1109/ROBOT.2003.1242016.

[37] Feleke AG, Bi L, Fei W. “EMG-Based 3D Hand Motor Intention Prediction for Information Transfer from Human to Robot”. Sensors (Basel). 2021 Feb 12;21(4):1316. doi: 10.3390/s21041316. PMID: 33673141; PMCID: PMC7918055.

[38] A. Dwivedi, G. Gorjup, Y. Kwon and M. Liarokapis, "Combining Electromyography

and Fiducial Marker Based Tracking for Intuitive Telemanipulation with a Robot Arm Hand System," 2019 28th IEEE International Conference on Robot and Human Interactive Communication (RO-MAN), 2019, pp. 1-6, doi: 10.1109/RO-MAN46459.2019.8956456.

[39] M. Shahbazi, S. F. Atashzar and R. V. Patel, "A Systematic Review of Multilateral Teleoperation Systems," in IEEE Transactions on Haptics, vol. 11, no. 3, pp. 338-356, 1 July-Sept. 2018, doi: 10.1109/TOH.2018.2818134.

[40] Yaqoob M, Sher Qaisrani SR, Waqas Tariq M, Ayaz Y, Iqbal S, Nisar S. "Design and Control of a Haptic Enabled Robotic Manipulator". International Journal of Advanced Robotic Systems. 2015;12(7). doi:10.5772/61039

[41] U. Kim, D. -H. Lee, W. J. Yoon, B. Hannaford and H. R. Choi, "Force Sensor Integrated Surgical Forceps for Minimally Invasive Robotic Surgery," in IEEE Transactions on Robotics, vol. 31, no. 5, pp. 1214-1224, Oct. 2015, doi: 10.1109/TRO.2015.2473515.

[42] Den Boer, K., Herder, J., Sjoerdsma, W. *et al.* "Sensitivity of laparoscopic dissectors". *Surg Endosc* **13**, 869–873 (1999).

[43] Hollinger, Avrum & Wanderley, Marcelo. (2011). "Evaluation of Commercial Force-Sensing Resistors".

[44] Min Li, Jelizaveta Konstantinova, and Kaspar Althoefe "Haptic Feedback Modalities for Minimally Invasive Surgery", 07 June 2018.

[45] J. Fernandes, J. Chen and H. Jiang, "Three-Axis Capacitive Sensor Arrays for Local and Global Shear Force Detection," in Journal of Microelectromechanical Systems, vol. 30, no. 5, pp. 799-813, Oct. 2021, doi: 10.1109/JMEMS.2021.3101735.

[46] Interlink Electronics (2022), FSR400 Datasheet, https://www.alldatasheet.com/view.jsp?Searchword=Fsr400%20datasheet&gad=1&gclid=Cj0KCQjwyLGjBhDKARIsAFRNgW_ZK6nbe2pOYMQL7gjCIx8ssZMNPDxvEvLgeWq1wJNfzY9EERtN_bMaAh_5EALw_wcB

[47] J. A. Flórez and A. Velásquez, "Calibration of force sensing resistors (fsr) for static and dynamic applications," 2010 IEEE ANDESCON, Bogota, Colombia, 2010, pp. 1-6, doi: 10.1109/ANDESCON.2010.5633120.

[48] Oyedotun, Kabir. (2018). "Synthesis and characterization of carbon-based nanostructured material electrodes for designing novel hybrid supercapacitors." 10.13140/RG.2.2.20007.50084.

[49] "Copper Foil Tape 1126 with Electrically Conductive Acrylic Adhesive" Datasheet 3M

[50] (2021) Smooth-On website. [Online]. Available: https://www.smooth-on.com/products/Ecoflex00-_30/

[51] (2020) INeed website. [Online]. Available: https://www.ineedmotors.com/news/erms-eccentricrotating-mass-vibration-motors-34485553.html

[52] (2020) Leader website. [Online]. Available: **https://www.leader-w.com/3v-8mm-flatvibrating-mini-electric-motor.html**

[53] Espressif (2022), ESP32 Datasheet, https://www.espressif.com/sites/default/files/documentation/esp32-wroom-32e_esp32-wroom-32ue_datasheet_en.pdf

[54] Sung-Kyun Kim, Won-Ho Shin, Seong-Young Ko, Jonathan Kim and Dong-Soo Kwon, "Design of a compact 5-DOF surgical robot of a spherical mechanism: CURES," 2008 IEEE/ASME International Conference on Advanced Intelligent Mechatronics, Xian, 2008, pp. 990-995, doi: 10.1109/AIM.2008.4601796.

[55] R.S. Popović, Hall-effect devices, Sensors and Actuators, Volume 17, Issues 1–2, 1989, Pages 39-53, ISSN 0250-6874, https://doi.org/10.1016/0250-6874(89)80063-0

[56] AMS AS5600: 12-Bit Programmable Magnetic Rotary Position Sensor Datasheet. Retrieved from https://ams.com/documents/20143/36005/AS5600_DS000365_5-00.pdf

[57] Texas Instruments. (n.d.). ADS1115: 16-Bit Analog-to-Digital Converter with Programmable Gain Amplifier. Retrieved from https://www.ti.com/lit/ds/symlink/ads1115.pdf

[58] Analog Devices, Sigma-Delta tutorial, retrieved form: https://www.analog.com/en/design-center/interactive-design-tools/sigma-delta-adc-tutorial.html

[59] Texta Instrument, Three guidelines for designing Anti-Aliasing Filters (AAF), retrieved from: https://e2e.ti.com/blogs_/archives/b/precisionhub/posts/three-guidelines-for-designing-anti-aliasing-filters

[60] Analog Devices, Inc. (n.d.). AD7746: 24-Bit Capacitance-to-Digital Converter. Retrieved from (https://www.alldatasheet.com/view.jsp?Searchword=Ad7746&gclid=CjwKCAjw67ajBhAVEiwA2g_jEDQFfp22ZiLecMXrarmllQWXTwH7GZvSkkOg1x3XzTpuM5NoNuAsohoCGSUQAvD_BwE)

[61] THECODEPROGRAM, I2C communication, and Connect 5 Arduinos with I2C, retrieved form: https://thecodeprogram.com/i2c-communication-and-connect-5-arduinos-with-i2c

[62] Components101, FTDI Converter module, retrieved from: https://components101.com/modules/ft232rl-usb-to-ttl-converter-pinout-features-datasheet-working-application-alternative